J. Plasma Phys. (2023), *vol*. 89, 905890408
Published by Cambridge University Press

doi:10.1017/S0022377823000612

Quasilinear theory of Brillouin resonances in rotating magnetized plasmas

J.-M. Rax [1,2], **R. Gueroult** [3,†] **and N.J. Fisch** [4]

[1] Andlinger Center for Energy + the Environment, Princeton University , Princeton, NJ 08540, USA

[2] IJCLab, Université de Paris-Saclay , 91405 Orsay, France

[3] LAPLACE, Université de Toulouse, CNRS, INPT, UPS , 31062 Toulouse, France

[4] Department of Astrophysical Sciences, Princeton University , Princeton, NJ 08540, USA

(Received 4 May 2023; revised 13 June 2023; accepted 14 June 2023)

Both spin and orbital angular momentum can be exchanged between a rotating wave and a rotating magnetized plasma. Through resonances the spin and orbital angular momentum of the wave can be coupled to both the cyclotron rotation and the drift rotation of the particles. It is, however, shown that the Landau and cyclotron resonance conditions which classically describe resonant energy–momentum exchange between waves and particles are no longer valid in a rotating magnetized plasma column. In this case a new resonance condition which involves a resonant matching between the wave frequency, the cyclotron frequency modified by inertial effects and the harmonics of the guiding centre rotation is identified. A new quasilinear equation describing orbital and spin angular momentum exchanges through these new Brillouin resonances is then derived, and used to expose the wave-driven radial current responsible for angular momentum absorption.

Key words: plasma dynamics, plasma nonlinear phenomena, plasma waves

1. Introduction

Understanding how to sustain and control the angular momentum of a rotating magnetized plasma column is a central issue, both for applied and basic plasma physics. On the former, the first successful application of rotating non-neutral plasmas was the magnetron microwave source theorized by Brillouin (1945). Since then, an important motivation for rotating plasma configurations has been and continues to be thermonuclear fusion (Lehnert 1971), both with rotating tokamaks (Ochs & Fisch 2017; Rax, Gueroult & Fisch 2017) and rotating mirrors (Bekhtenev *et al.* 1980; Hassam 1997; Fetterman & Fisch 2008, 2010; Teodorescu *et al.* 2010). Besides fusion, rotating plasmas have also attracted attention for ion acceleration (Janes 1965; Janes, Levy & Petschek 1965; Janes *et al.* 1966) and mass separation (Bonnevier 1966; Krishnan, Geva & Hirshfield 1981; Prasad & Krishnan 1987) as envisioned for instance for nuclear waste cleanup (Gueroult, Hobbs & Fisch 2015), spent nuclear fuel reprocessing (Gueroult & Fisch 2014; Timofeev

† Email address for correspondence: renaud.gueroult@laplace.univ-tlse.fr

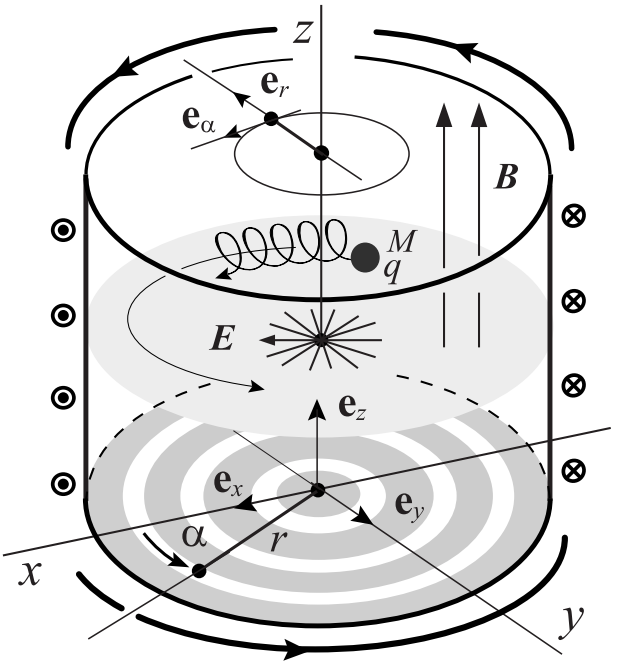

FIGURE 1. Electric and magnetic fields configurations in a plasma rotating around the z axis, α is the polar angle and r the polar radius.

2014; Vorona *et al.* 2015; Dolgolenko & Muromkin 2017) or rare earth element recycling (Gueroult, Rax & Fisch 2018). On the latter, magnetized rotating plasma theory has been shown to be important in understanding pulsar dynamics and radiative transfer (Gueroult *et al.* 2019*b*), rotation augmented gyrotropy (Gueroult, Rax & Fisch 2020) or image rotation (aka Faraday–Fresnel effect) in plasmas (Rax & Gueroult 2021). The adiabatic theory of angular momentum perturbation in rotating magnetized plasmas also provides an interesting realization of a geometrical Berry type phase (Rax & Gueroult 2019).

Two fields configurations can sustain the steady state rotation of a magnetized plasma. One is the Hall configuration with a radial magnetic field and an axial electric field. This is the configuration used notably in stationary plasmas thrusters. The other, illustrated in figure 1, is the Brillouin configuration with an axial magnetic field and a radial electric field. This is the configuration used notably in mass separators (Gueroult *et al.* 2019*c*) and homopolar devices (Barber, Swift & Tozer 1972). In this study we will restrict our analysis to this last configuration and study the quasilinear theory of angular momentum exchange between waves and particles in a rotating Brillouin configuration.

Steady state angular momentum injection to compensate dissipation in a rotating cylindrical magnetized plasma column is usually envisioned through the use of concentric annular direct current (DC) biased end-electrodes, as illustrated in grey in figure 1. This is the scheme originally proposed by Lehnert (Lehnert 1970, 1973), where electrodes are assumed to drive a DC radial electric field perpendicular to the DC axial magnetic field. It has, however, been recently shown that field penetration through the sheath and along field lines imposes a number of constraints on the achievable electric field (Gueroult, Rax & Fisch 2019*a*; Poulos 2019; Liziakin, Gavrikov & Smirnov 2020; Liziakin *et al.* 2021; Trotabas & Gueroult 2022). Meanwhile, studies in the last decade on rotating mirrors (Fetterman & Fisch 2008, 2010) and rotating tokamaks (Ochs & Fisch 2017; Rax *et al.*

https://doi.org/10.1017/S0022377823000612 Published online by Cambridge University Press

2017) have underlined the potential to use electromagnetic waves to drive plasma rotation through resonant wave–particle angular momentum absorption, and to compensate for dissipative relaxation. Although very promising, these studies relied on a simple photon picture.

The standard tool to study resonant wave–particle interaction is the quasilinear theory. For an infinite homogeneous magnetized plasma at rest the quasilinear equation is well known (Rax 2011), and has proven particularly useful to evaluate energy absorption and current generation in thermonuclear plasmas (Fisch 1978, 1987). The quasilinear equation for a cylindrical unmagnetized plasma at rest has also been derived (Kaufman 1971), whereas a generalized quasilinear theory for inhomogeneous plasma has recently been laid out (Dodin 2022). However, and while as mentioned above it appears to be key to important applications, the quasilinear theory for a rotating magnetized plasma has to our knowledge not been derived yet. While quasilinear radial transport has been studied within the framework of non-neutral plasmas confinement deploying a so-called 'rotating wall technique' (Eggleston & O'Neil 1999; Kiwamoto, Soga & Aoki 2005), these studies were restricted to electrostatic modes. Finite Larmor radius effects were also neglected as an infinite magnetic field was assumed. Lastly, although inertial effects are central to equilibria in Brillouin configurations, these studies neglected inertial effects so that the resonance condition is limited to the axial Doppler-shifted resonance between the plasma rotation and the wave frequency. These restrictions are removed in the present paper. Here we derive the quasilinear equation for a rotating wave and a rotating magnetized plasma, which describes angular momentum absorption/emission within a kinetic framework, and use it to uncover the interplay between orbital angular momentum (OAM), spin angular momentum (SAM) and finite Larmor radius (FLR) effects.

This paper is organized as follows. We begin by recalling in § 2 basic elements on wave and particle angular momentum. We then proceed to derive in § 3 the Hamiltonian description of a magnetized rotating plasma sustained by a radial electric field, and to expose the physical and geometrical meaning of the angle–action variables used to describe the particle dynamics. These canonical angle–action variables are after that used to identify the relation between the canonical and the kinetic angular momentum in § 4, and to model as a perturbed Hamiltonian the effect of a rotating wave perturbation on the rotating particle dynamics in § 5. This formalism is then used to identify a new resonance condition in § 6, and to derive the quasilinear kinetic equation describing the time evolution of the distribution function in action space in § 7. This new kinetic equation is finally used to study OAM and SAM absorption in § 8, and to derive the expression of the wave-driven radial current in § 9. Lastly, § 10 concludes this study and summarizes the main findings.

2. Wave and particle angular momentum

In the following we use (r, α, z), a set of cylindrical coordinates on a cylindrical basis $(\boldsymbol{e}_r, \boldsymbol{e}_\alpha, \boldsymbol{e}_z)$. The associated set of Cartesian coordinates is (x, y, z) on the Cartesian basis $(\boldsymbol{e}_x, \boldsymbol{e}_y, \boldsymbol{e}_z)$. The vertical axis along z is the direction of the background static magnetic field $\boldsymbol{B} = B\boldsymbol{e}_z$ and the DC electric field $\boldsymbol{E} = E\boldsymbol{e}_r$ is along the radial direction. This is the configuration illustrated in figure 1.

Electromagnetic waves can carry both SAM – associated with right-hand (R) and left-hand (L) circular polarizations – and OAM (Gough 1986; Barnett & Allen 1994; van Enk & Nienhuis 1994; Götte, Barnett & Padgett 2007; Barnett, Babiker & Padgett 2017). The vector field of such a wave has a helical phase front structure and can in general be

https://doi.org/10.1017/S0022377823000612 Published online by Cambridge University Press

written as

$$\mathrm{Re}\left[\frac{\boldsymbol{e}_x \pm j\boldsymbol{e}_y}{\sqrt{2}}\mathcal{E}_\pm(r)\exp j\,(n\alpha + \beta z - \omega t)\right]. \tag{2.1}$$

Here $(\boldsymbol{e}_x + j\boldsymbol{e}_y)\mathcal{E}_+$ is a R circularly polarized field while $(\boldsymbol{e}_x - j\boldsymbol{e}_y)\mathcal{E}_-$ is a L circularly polarized field, the electric field $\mathcal{E}(r)$ is the solution of the radial part of Maxwell's equations, ω is the wave frequency, $n \in \mathbb{Z}$ is the azimuthal mode number and $\beta \in \mathbb{R}$ is the axial wavevector. An observer located at a fixed point (r_0, α_0, z_0) and probing azimuthally the electric field amplitude $|\mathcal{E}_\pm(r_0)|$ of the wave described by (2.1) will measure a field pattern $|\mathcal{E}_\pm(r_0)|$ rotating at the angular velocity $\mathrm{d}\alpha/\mathrm{d}t = \omega/n$. The formal identification of SAM and OAM contents for the wavevector field given in (2.1), as well as the definition of the associated SAM and OAM operators $\hat{\boldsymbol{S}}$ and $\hat{\boldsymbol{L}}$, are discussed in Appendix A. Plasma waves carrying OAM has been an active research topic in the last decade, both in unmagnetized (Mendonça 2012; Chen, Qin & Liu 2017; Bliokh & Bliokh 2022) and magnetized (Shukla 2012; Stenzel & Urrutia 2015; Stenzel 2016) plasmas.

Meanwhile, magnetized charged particles in axisymmetric fields can also carry both SAM and OAM. The former is associated with the cyclotron motion while the latter is associated with the guiding centre motion around the z axis. Note that for classical particles, the separation of angular momentum into cyclotron SAM and drift OAM does not arise from a quantum analysis. It is a simple application of Koenig's theorem which states that the angular momentum of a system can be decomposed into an external orbital part and an internal part. This internal part is nowadays called the spin part for waves and magnetized charges, even within a classical framework. Note also that while the quantum SAM of the charged particles $\pm\hbar/2$ should in principle be considered along with the cyclotron SAM and the drift OAM, it will be neglected in this study as the plasma temperature is assumed to be far larger than $\hbar\omega_c$ which is of the order of 10^{-7} eV for protons and a magnetic field of 1 T. Consider now more specifically the plasma column shown in figure 1 with a background axial magnetic field $\boldsymbol{B} = B\boldsymbol{e}_z$ and a radial electric field $\boldsymbol{E} = E\boldsymbol{e}_r$, which leads to a guiding centre $E \times B$ rotation around the z axis. An ion with charge q and mass M is described by (i) its instantaneous position $\boldsymbol{r} = \boldsymbol{R}_G + \boldsymbol{\rho}_L$, where $\boldsymbol{R}_G$ is the guiding centre position and $\boldsymbol{\rho}_L(t)$ the Larmor radius, and (ii) its velocity $\boldsymbol{v} = \boldsymbol{V}_G + \boldsymbol{v}_c$, where $\boldsymbol{V}_G \sim (E/B)\boldsymbol{e}_\alpha$ is the guiding centre drift velocity and $\boldsymbol{v}_c(t) = \omega_c\boldsymbol{e}_z \times \boldsymbol{\rho}_L$ is the cyclotron velocity with $\omega_c = qB/M$ the ion cyclotron frequency. The instantaneous angular momentum is defined as $M\boldsymbol{r} \times \boldsymbol{v}$ and its average $\langle\ \rangle$ over the fast cyclotron motion is

$$M\langle(\boldsymbol{R}_G + \boldsymbol{\rho}_L) \times (\boldsymbol{V}_G + \boldsymbol{v}_c)\rangle \cdot \boldsymbol{e}_z = MR_G^2\varpi + M\rho_L^2\omega_c = L_z + S_z, \tag{2.2}$$

where $\varpi = (E/BR_G)$ is the angular $E \times B$ drift velocity. The OAM part of (2.2) is $L_z = M_G\varpi$ with $M_G = MR_G^2$ the guiding centre moment of inertia of the ion with respect to the z axis. The cyclotron spin part S_z is defined as $(2M/q)\mu$ with $\mu = m\omega_c^2\rho_L^2/2B$ the Larmor magnetic moment. One thus recovers the classical gyromagnetic factor $q/2M$.

Coupling between wave and particle angular momentum components introduced above can be either adiabatic or resonant. At the fluid level, linear adiabatic coupling is described by the Hermitian part of the dielectric tensor, while linear resonant coupling is described by the anti-Hermitian part of the dielectric tensor and the quasilinear equation. Starting with adiabatic coupling, coupling between wave SAM and particles SAM leads to the classical Faraday rotation (Chen 1984; Rax 2005). Adiabatic coupling between wave SAM and particles OAM leads to the mechanical Faraday – or polarization drag (Jones 1976) – effect whose properties in plasmas have recently been examined (Gueroult *et al.* 2019*b*, 2020). Lastly, adiabatic coupling between wave OAM and particles OAM leads

https://doi.org/10.1017/S0022377823000612 Published online by Cambridge University Press

to the Faraday–Fresnel rotation and splitting recently uncovered for Trievelpiece–Gould and helicon modes (Rax & Gueroult 2021). Moving on to resonant coupling, coupling between wave SAM and particles SAM is routinely used for electron and ion cyclotron resonance heating (ECRH/ICRH) in tokamaks (Rax 2011), and has also been proposed for mass separation or particle acceleration (Loeb & Friedland 1986; Pendergast *et al.* 1988; Rax, Robiche & Fisch 2007; Rax & Robiche 2010). Meanwhile, as already mentioned in the introduction, resonant coupling between wave OAM and particles OAM has been proposed to control rotation in magnetic mirrors (Fetterman & Fisch 2008, 2010) and tokamaks (Ochs & Fisch 2017; Rax *et al.* 2017).

In this study we will build on and extend these results by deriving the quasilinear kinetic equation which will allow us to identify the exact resonance condition, and from there to uncover couplings between waves and particles SAM and OAM, in a cylindrical rotating magnetized plasma. This new resonance condition completes the already identified set of resonant coupling in plasmas: (i) Landau in unmagnetized plasmas; (ii) cyclotron in magnetized plasmas; and (iii) Compton in laser-driven plasmas (Rax 1992). Because our motivation is primarily in rotating mirrors, straight tokamaks and mass filters where the resonant population is the ion population, we will consider a non-relativistic framework. Under this assumption, we will show that FLR effects are responsible for a mixing of OAM and SAM couplings, underlining that rotating magnetized plasmas feature a more complex angular momentum dynamics than unmagnetized plasmas or ordinary neutral matter.

3. Hamiltonian description of a rotating plasma

In this section we lay out the Hamiltonian description of an unperturbed rotation driven by a DC radial electric field in an axially magnetized plasma column. The axial magnetic field is assumed to be produced by a set of coils carrying azimuthal DC currents at the edge of the plasma column. The radial electric field may be generated through DC polarized concentric electrodes at ends of the plasma, provided that the criterion for electric field penetration is fulfilled (Gueroult *et al.* 2019*a*; Poulos 2019; Liziakin *et al.* 2020, 2021; Trotabas & Gueroult 2022). Alternatively, in a non-neutral plasma (Davidson 2001), the electric field is simply the space charge field and there is no need for concentric electrodes. We focus on the ion population in a quasineutral plasma but results can be easily extended to the electron population in quasineutral and non-neutral plasmas.

3.1. *Brillouin modes*

An ion of mass M and charge $q > 0$, interacts with a static radial linear electric field $\boldsymbol{E}$ and an axial uniform magnetic field $\boldsymbol{B}$ as shown in figure 1 and defined by

$$\frac{q}{M}\boldsymbol{E} = \left(\frac{qE}{Mr}\right) r\boldsymbol{e}_r, \tag{3.1}$$

$$\frac{q}{M}\boldsymbol{B} = \omega_c \boldsymbol{e}_z. \tag{3.2}$$

Ion orbits are then a combination of the slow and fast Brillouin rotations (Davidson & Krall 1969; Davidson 2001). The fast Ω_+ and slow Ω_- angular velocities associated with these fast and slow rotations are given by

$$\Omega_\pm = -\frac{\omega_c}{2} \mp \sqrt{\frac{\omega_c^2}{4} - \frac{qE}{rM}} \underset{|\frac{E}{rB}| \ll \omega_c}{\approx} -\frac{\omega_c}{2} \mp \frac{\omega_c}{2} \pm \frac{E}{rB}, \tag{3.3}$$

where E is the DC radial electric field at a given radius r and $4qE < Mr\omega_c^2$ is the classical Brillouin condition (Davidson 2001). These two solutions are plotted as a function of

https://doi.org/10.1017/S0022377823000612 Published online by Cambridge University Press

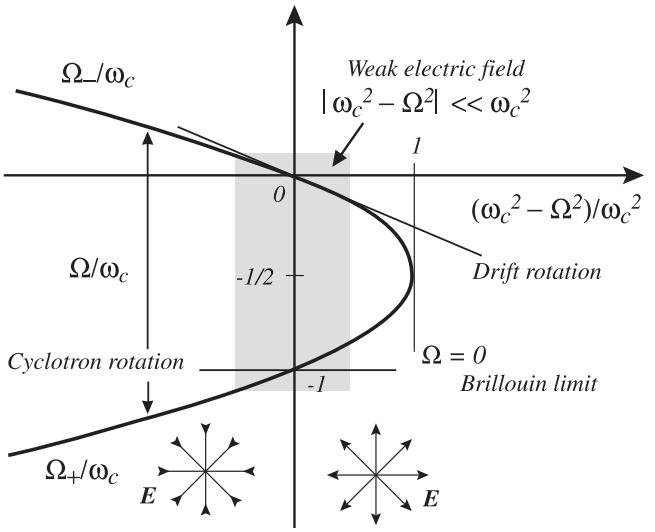

FIGURE 2. The slow and fast angular velocity as a function of the electric field. A clear separation between guiding centre and Larmor radius is relevant for weak electric field in the grey zone.

the normalized electric field in figure 2. In the weak electric field regime $|E/(rB)| \ll \omega_c$ highlighted in grey in figure 2, the angular velocity of the guiding centre around the z axis reduces to the classical $E \times B$ drift while the angular velocity of the cyclotron motion around the guiding centre reduces to the usual cyclotron motion. This corresponds to the asymptotic limit on the right-hand side of (3.3).

From (3.1) the Brillouin limit leads to the simple requirement $\Omega^2 > 0$ with

$$\Omega = \sqrt{\frac{q^2B^2}{M^2} - 4\frac{qE}{Mr}}. \tag{3.4}$$

Note that Ω, the gyrofrequency ω_c and the wave frequency ω are all assumed positive throughout this study. Another way to see the condition $\Omega > 0$ is to realize that for a given field configuration ((3.1) and (3.2)) the cutoff mass M^* between radially unconfined and radially confined ions is the solution of $\Omega^2(M^*) = 0$. Ions such that $M < M^*$ remain confined around the axis of the configuration. On the other hand ions such that $M > M^*$ are expelled radially at an exponential rate. The assumption in this study of $M < M^*$ or $\Omega > 0$ is thus a requirement to study radially bounded trochoidal orbits.

With the definition of Ω in (3.4) the usual slow and fast Brillouin modes given by (3.3) rewrite as

$$\Omega_\pm = -\frac{\omega_c \pm \Omega}{2}. \tag{3.5}$$

One verifies that $\Omega_+ + \Omega_- = -\omega_c$ and $\Omega_+ - \Omega_- = -\Omega$. Note also that $\Omega_+ < 0$ and $\nabla \cdot \boldsymbol{E} = 2\Omega_+\Omega_-$. The uniform charge density $2\varepsilon_0 M\Omega_+\Omega_-/q$ is the small deviation from quasineutrality responsible for the radial electric field.

3.2. *Hamiltonian description*

Consider now a system of units such that $q = 1$ and $M = 1$. In this simple system of units, the electric field and the magnetic field given in (3.1) and (3.2) derive, respectively, from

https://doi.org/10.1017/S0022377823000612 Published online by Cambridge University Press

the scalar potential

$$\Phi = \frac{\Omega^2 - \omega_c^2}{8}(x^2 + y^2) \tag{3.6}$$

and the vector potential

$$\boldsymbol{A} = \frac{\omega_c}{2}(x\boldsymbol{e}_y - y\boldsymbol{e}_x). \tag{3.7}$$

The unperturbed Hamiltonian H_0 is classically the sum of the kinetic energy $\boldsymbol{v}^2/2$ plus the potential energy $\Phi(\boldsymbol{r})$, that is

$$H_0(\boldsymbol{p}, \boldsymbol{r}) = \tfrac{1}{2}\boldsymbol{v}^2 + \Phi = \tfrac{1}{2}[\boldsymbol{p} - \boldsymbol{A}(\boldsymbol{r})]^2 + \Phi(\boldsymbol{r}), \tag{3.8}$$

where $\boldsymbol{v}$ is the velocity and $\boldsymbol{p} = p_x\boldsymbol{e}_x + p_y\boldsymbol{e}_y + p_z\boldsymbol{e}_z$ is the canonical momentum conjugated to the position $\boldsymbol{r} = x\boldsymbol{e}_x + y\boldsymbol{e}_y + z\boldsymbol{e}_z$ of the ion. In Cartesian coordinates (3.8) rewrites as

$$H_0 = \frac{1}{2}(p_x^2 + p_y^2) + \frac{\omega_c}{2}(yp_x - xp_y) + \frac{\Omega^2}{8}(x^2 + y^2) + \frac{p_z^2}{2}. \tag{3.9}$$

This is a quadratic form of the Cartesian momentum and positions variables, so that H_0 is integrable (Rax 2021).

Let us now introduce the canonical change of variables from the old Cartesian momentum $(p_x, p_y, p_z = P)$ and positions (x, y, z) to the new actions (J, D, P) and angles (φ, θ, z) variables defined by

$$x = \sqrt{\frac{2D}{\Omega}}\cos\theta - \sqrt{\frac{2J}{\Omega}}\cos\varphi, \quad y = \sqrt{\frac{2D}{\Omega}}\sin\theta + \sqrt{\frac{2J}{\Omega}}\sin\varphi, \tag{3.10a,b}$$

$$p_x = -\sqrt{\frac{\Omega D}{2}}\sin\theta + \sqrt{\frac{\Omega J}{2}}\sin\varphi, \quad p_y = \sqrt{\frac{\Omega D}{2}}\cos\theta + \sqrt{\frac{\Omega J}{2}}\cos\varphi, \tag{3.11a,b}$$

with $J \geq 0$, $D \geq 0$, $\varphi \in [0, 2\pi]$ and $\theta \in [0, 2\pi]$. By plugging (3.10*a*,*b*) and (3.11*a*,*b*) into (3.9) one simply gets

$$H_0 = -\Omega_+ J + \Omega_- D + \tfrac{1}{2}P^2. \tag{3.12}$$

This result is independent of the angles (φ, θ, z) as expected. Note also from (3.5) that the cyclotron (kinetic) part of the energy $-\Omega_+ J$ is always positive, but that the drift (potential) part $\Omega_- D$ can be either positive or negative. The particle velocity perpendicular to the magnetic field $\boldsymbol{v}$ defined as $p_x\boldsymbol{e}_x + p_y\boldsymbol{e}_y - \boldsymbol{A}$ and the polar radius r defined as $\sqrt{x^2 + y^2}$ are then obtained from a simple substitution of (3.10*a*,*b*) and (3.11*a*,*b*) in the Cartesian definitions, leading to

$$\begin{aligned}\boldsymbol{v} = &\left(-\Omega_+\sqrt{\frac{2J}{\Omega}}\sin\varphi - \Omega_-\sqrt{\frac{2D}{\Omega}}\sin\theta\right)\boldsymbol{e}_x \\ &+ \left(-\Omega_+\sqrt{\frac{2J}{\Omega}}\cos\varphi + \Omega_-\sqrt{\frac{2D}{\Omega}}\cos\theta\right)\boldsymbol{e}_y\end{aligned} \tag{3.13}$$

and

$$r^2 = x^2 + y^2 = 2\frac{J + D}{\Omega} - 4\frac{\sqrt{JD}}{\Omega}\cos(\theta + \varphi). \tag{3.14}$$

Having identified a set of canonical angles (φ, θ, z) and actions (J, D, P) variables describing the ion interaction with the electric and magnetic field given in (3.6) and (3.7),

https://doi.org/10.1017/S0022377823000612 Published online by Cambridge University Press

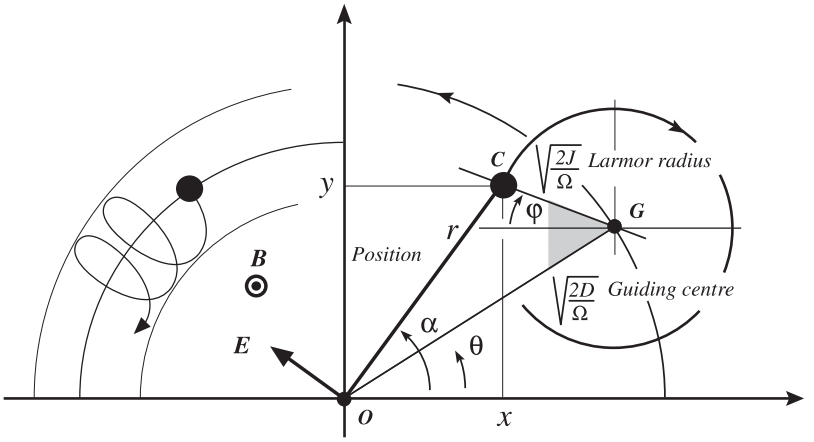

FIGURE 3. Physical meaning of the angle (φ, θ) and actions $(J < D)$ variables in real (x, y) space.

we can now try to shed light onto the physical meaning of the new variables. Starting with z and P, they are, respectively, the usual Cartesian coordinate and momentum $P = Mv_z$, and their physical interpretation is thus straightforward. The meaning of (J, φ) and (D, θ) is on the other hand less obvious. To help our interpretation, figure 3 shows the ion motion in the (x, y) plane when $D > J$. The instantaneous position of the ion is $\boldsymbol{r} = r\boldsymbol{e}_r = \boldsymbol{OC}$ and it can be viewed as the sum of a rotating Larmor radius $\boldsymbol{GC}$ plus a rotating guiding centre $\boldsymbol{OG}$. From figure 3, θ is the anticlockwise angle between $\boldsymbol{e}_x$ and $\boldsymbol{OG}$, and φ is the clockwise angle between $-\boldsymbol{e}_x$ and $\boldsymbol{GC}$. We then find from (3.10*a*,*b*) that the guiding centre $|\boldsymbol{OG}| = \sqrt{2D/\Omega}$, and that the Larmor radius $|\boldsymbol{GC}| = \sqrt{2J/\Omega}$. Equation (3.14) is just the law of cosines applied to the $\boldsymbol{OGC}$ triangle with respect to the grey angle in figure 3.

The geometrical interpretation proposed above for (J, φ) and (D, θ) based on figure 3 assumed $D > J$. If one now considers $J > D$, the canonical description ((3.10*a*,*b*)–(3.12)) is still valid, but the picture of the orbit is to be replaced by the one shown in figure 4. As we will show in the next section these two regimes $J \lessgtr D$ can be discriminated based on the sign of the particle canonical angular momentum. In effect most of the physical interpretations made in this study will be argued with the ordering $D > J$ in mind as it is the most intuitive, but one should keep in mind that all the relations are valid in both cases $J \lessgtr D$.

Finally, one verifies that Hamilton's equations

$$\frac{\mathrm{d}\theta}{\mathrm{d}t} = \frac{\partial H_0}{\partial D} = \Omega_-, \quad \frac{\mathrm{d}\varphi}{\mathrm{d}t} = \frac{\partial H_0}{\partial J} = -\Omega_+, \tag{3.15a,b}$$

lead to the expected classical Brillouin results (Davidson 2001). The minus sign for the fast (cyclotron) rotation is simply due to the choice of a clockwise angle for φ (the anticlockwise choice for θ). It must be stressed here though that the Larmor radius angle φ does not rotate at the cyclotron frequency $-\Omega_+ \neq \omega_c$. Similarly the θ angle of the guiding centre does not rotate with the $E \times B$ velocity $\Omega_- \neq -E_r/rB$. This is the consequence of inertial effects. The interpretation of the motion as a slow $E \times B$ drift $\Omega_- \approx -E_r/rB$ plus a fast cyclotron rotation $\Omega_+ \approx -\omega_c$ is thus only meaningful in the weak electric field limit $|E_r/B| \ll r\omega_c$ highlighted in grey in figure 2.

https://doi.org/10.1017/S0022377823000612 Published online by Cambridge University Press

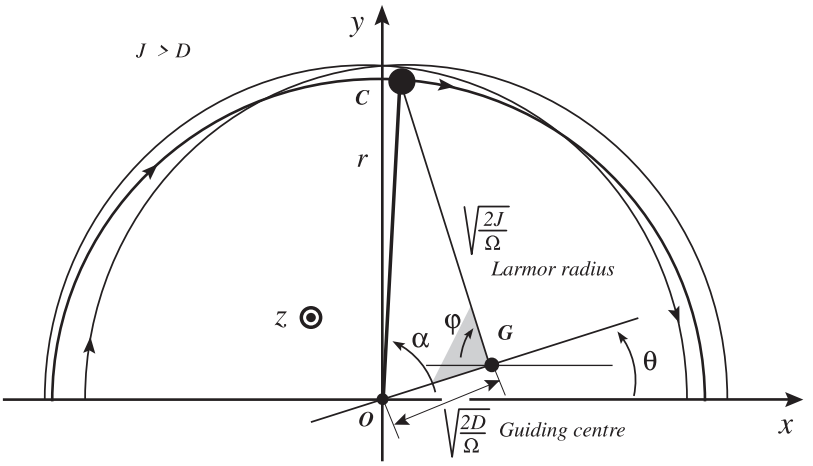

FIGURE 4. Physical meaning of the angle (φ, θ) and actions $(J > D)$ variables in real (x, y) space.

3.3. *Weak field limit*

In order to develop a deeper physical understanding of the weak field regime, which is the one of experimental interest for quasineutral plasmas applications, let us write the ion orbit as a combination of an $E \times B$ slow rotation plus a fast cyclotron rotation. We introduce the guiding centre radius R_G and the Larmor radius ρ_L:

$$x = R_G \cos\left(-\frac{E}{rB}t\right) - \rho_L \cos(\omega_c t), \tag{3.16}$$

$$y = R_G \sin\left(-\frac{E}{rB}t\right) + \rho_L \sin(\omega_c t). \tag{3.17}$$

Equations (3.16) and (3.17) are simply a rewriting of (3.10*a*,*b*) in the weak field limits $|E_r/rB| \ll \omega_c$. In this weak field limit $\Omega \approx \omega_c$, and the actions J and D can be, respectively, related to the cyclotron orbit magnetic flux $\Psi_L = \pi\rho_L^2 B$ and the guiding centre orbit magnetic flux $\Psi_G = \pi R_G^2 B$, with

$$D \approx \frac{\omega_c}{2} R_G^2 = \frac{\Psi_G}{2\pi}, \tag{3.18}$$

$$J \approx \frac{\omega_c}{2} \rho_L^2 = \frac{\Psi_L}{2\pi}. \tag{3.19}$$

Note that these two magnetic fluxes are the first and third adiabatic invariant of Alfven's theory. The usual link between action variables and adiabatic invariants is thus recovered.

Assuming further $J \ll D$, that is a small Larmor radius, and reintroducing momentarily the ion mass and charge M and q for clarity, one gets in the weak field regime

$$-\Omega_+ J \approx \frac{M}{2} v_c^2, \tag{3.20}$$

$$\Omega_- D \approx q\Phi\,(R_G) + \frac{M}{2}\frac{E^2}{B^2}. \tag{3.21}$$

https://doi.org/10.1017/S0022377823000612 Published online by Cambridge University Press

Plugging these results into (3.12) yields

$$H_0 \underset{|\frac{E}{rB}|\ll\omega_c}{\approx} \frac{M}{2}v_c^2 + \frac{1}{2M}P^2 + \frac{M}{2}\frac{E^2}{B^2} + q\Phi. \tag{3.22}$$

The Hamiltonian thus reduces in this limit to the sum of four terms: the cyclotron kinetic energy $Mv_c^2/2$; the electrostatic potential energy $q\Phi(R_G)$ of the guiding centre; the drift energy $ME^2/2B^2$; and the parallel kinetic energy .

If one considers now a wave perturbation δH_0 of the Hamiltonian H_0, (3.22) shows that in the weak field limit this perturbation is associated with an increase or a decrease of (i) the kinetic cyclotron energy $Mv_c\delta v_c$, (ii) the potential energy $q\delta\Phi$ and (iii) the axial kinetic energy $Mv_z\delta v_z$. The structure of the unperturbed Hamiltonian (3.12) indeed offers in this case the possibility to transfer axial linear momentum, kinetic energy $-\Omega_+\delta J \approx Mv_c\delta v_c$ or/and potential energy $\Omega_-\delta D \approx q\delta\Phi$ from rotating waves to rotating particles. When the weak field approximation is no longer valid, inertia effects make this picture more intricate, and the angle–action variables (φ, θ, z) and (J, D, P) then provide the right framework to understand the dynamics. In order to simplify the algebra, we define $\boldsymbol{J}$, $\boldsymbol{\theta}$ and $\boldsymbol{\Omega}$ such that

$$\boldsymbol{J} = (J, D, P), \tag{3.23}$$

$$\boldsymbol{\theta} = (\varphi, \theta, z), \tag{3.24}$$

$$\boldsymbol{\Omega} = \frac{\mathrm{d}\boldsymbol{\theta}}{\mathrm{d}t} = \frac{\partial H_0}{\partial \boldsymbol{J}} = (-\Omega_+, \Omega_-, P). \tag{3.25}$$

To conclude this section we note that as H_0 is integrable there exists an infinite set of canonical angle and action variables. The particular choice of $\boldsymbol{\theta}$ and $\boldsymbol{J}$ is simply motivated by their straightforward geometrical interpretation, as illustrated in figures 3 and 4, and their clear physical meaning in the weak field regime.

4. Canonical and kinetic angular momentum

From (3.10*a*,*b*), (3.11*a*,*b*) and (3.13)), the z components of the canonical angular momentum and of the kinetic angular momentum, respectively, write

$$L_C = xp_y - yp_x = D - J \tag{4.1}$$

and

$$L_K = xv_y - yv_x = \frac{2\Omega_-}{\Omega}D + \frac{2\Omega_+}{\Omega}J + \frac{2\omega_c}{\Omega}\sqrt{JD}\cos(\theta+\varphi)\,. \tag{4.2}$$

As noted in the previous section, the ordering of J and D depends on the sign of L_C. Specifically, $L_C > 0$ leads to the orbit topology illustrated in figure 3 while $L_C < 0$ leads to the orbit topology illustrated in figure 4. Note also that L_C is independent of time as a consequence of the cylindrical symmetry, but that L_K is a function of time since $\theta + \varphi = (\Omega_- - \Omega_+)t$.

A physical interpretation of (4.2) can be brought up by considering the moment of inertia of a rotating ion with mass $M = 1$. Seeing again the rotating ion as the sum of a rotating guiding centre and a rotating Larmor radius, the guiding centre moment of inertia is $M_G = 2D/\Omega$, while the Larmor radius moment of inertia is $M_L = 2J/\Omega$. The associated angular momenta are $M_G\,\mathrm{d}\theta/\mathrm{d}t = M_G\Omega_-$ (θ is anticlockwise) and $-M_L\,\mathrm{d}\varphi/\mathrm{d}t = M_L\Omega_+$ (φ is clockwise). One verifies that the sum of these two angular momenta $M_G\Omega_- + M_L\Omega_+$ indeed matches $\langle L_K\rangle$ computed from (4.2), where the average $\langle\rangle$ is over the angle $\theta + \varphi$.

https://doi.org/10.1017/S0022377823000612 Published online by Cambridge University Press

Defining the magnetic flux

$$\Psi = \oint_{\mathcal{C}} \boldsymbol{A} \cdot \mathrm{d}\,\boldsymbol{l} = \frac{\omega_c}{2} \oint (x\,\mathrm{d}y - y\,\mathrm{d}x) = \pi\omega_c r^2 \tag{4.3}$$

with $\mathcal{C}$ a contour along a $\Delta\alpha = 2\pi$ full turn of the orbit and r^2 given by (3.14), then (3.14), (4.1) and (4.2) can be further used to write

$$L_C = L_K + \frac{\Psi}{2\pi}. \tag{4.4}$$

We thus see that the criteria $L_C \lessgtr 0$, which was identified as determining the type of orbit topology (either that shown in figure 3 or that shown in figure 4), can be recast as $2\pi L_K \lessgtr -q\Psi$. This last condition can be interpreted as an ordering between the kinetic energy and the magnetic coupling.

5. Hamiltonian description of a rotating wave

We now consider a wave perturbation associated with a rotating and propagating potential

$$\phi\,(\boldsymbol{r}, t) = \mathrm{Re}[\phi(r) \exp j(n\alpha + \beta z - \omega t)], \tag{5.1}$$

and a R or L vector potential

$$\boldsymbol{a}_{\pm}\,(\boldsymbol{r}, t) = \mathrm{Re}\left[a\,(r) \exp j\,(n\alpha + \beta z - \omega t)\,\frac{\boldsymbol{e}_x \pm j\boldsymbol{e}_y}{\sqrt{2}}\right], \tag{5.2}$$

where $n \in \mathbb{Z}$ and $\beta \in \mathbb{R}$. The function $a(r)$ is the real amplitude solution of the radial part of Maxwell–Ampère equation. The Maxwell–Faraday equation is fulfilled through $\mathcal{E} = -\partial \boldsymbol{a}_{\pm}/\partial t$ and $\mathcal{B} = \boldsymbol{\nabla} \times \boldsymbol{a}$ where $\mathcal{E}$ and $\mathcal{B}$ are the wave electric and magnetic fields. The function $\phi(r)$ is the solution of Poisson equation. Such solutions of Maxwell–Ampère and Poisson equations were recently identified for the whistler or helicon branch and the Trievelpiece–Gould modes in a rotating plasma (Rax & Gueroult 2021). As shown in Appendix A, the wave $\boldsymbol{a}_{\pm}(\boldsymbol{r}, t)$ is both an SAM and OAM eigenfunction since

$$(\hat{L}_z + \hat{S}_z) \cdot \boldsymbol{a}_{\pm} = (n \mp 1)\,\boldsymbol{a}_{\pm}, \tag{5.3}$$

and the scalar potential wave $\phi(\boldsymbol{r}, t)$ is an OAM eigenfunction.

The perturbed Hamiltonian H describing the interaction of an ion with the DC confining fields ((3.6) and (3.7)) and the rotating RF waves ((5.1) and (5.2)) then writes as

$$H = \frac{1}{2}\,(\boldsymbol{p} - \boldsymbol{A})^2 + \Phi - (\boldsymbol{p} - \boldsymbol{A}) \cdot \boldsymbol{a}_{\pm} + \frac{\boldsymbol{a}_{\pm}^2}{2} + \phi. \tag{5.4}$$

In the following we neglect the second-order ponderomotive part of the interaction

$$\boldsymbol{a}_{\pm}^2/2 \ll \boldsymbol{v} \cdot \boldsymbol{a}_{\pm} \tag{5.5}$$

but keep the first-order dipolar coupling $\boldsymbol{v} \cdot \boldsymbol{a}_{\pm} + \phi$ which is responsible for the quasilinear resonant exchange of energy and momentum between waves and particles. This separation between dipolar and ponderomotive perturbations is usual and we will not explore here

https://doi.org/10.1017/S0022377823000612 Published online by Cambridge University Press

the interplay between these two couplings (Ochs & Fisch 2021*a*,*b*, 2022, 2023) which is associated with the transient build up of the wave. Defining

$$\boldsymbol{v}\cdot\boldsymbol{a}_{\pm}+\phi=v_x a_{\pm x}+v_y a_{\pm y}+\phi, \tag{5.6}$$

and assuming that $V_n \ll H_0$, we then write

$$H=H_0(\boldsymbol{J})+V_n(\boldsymbol{J},\boldsymbol{\theta},t), \tag{5.7}$$

that is that H is decomposed into an unperturbed part H_0 given in (3.12) and the wave perturbation. Using (3.13), (5.1) and (5.2), one gets for the wave perturbation

$$\begin{aligned} V_n=&\,\mathrm{Re}\left[\mp ja(r)\left[\Omega_+\sqrt{\frac{J}{\Omega}}\exp(\mp j\varphi)-\Omega_-\sqrt{\frac{D}{\Omega}}\exp(\pm j\theta)\right]\exp j(n\alpha+\beta z-\omega t)\right]\\ &+\mathrm{Re}\left[\phi(r)\exp j(n\alpha+\beta z-\omega t)\right]. \end{aligned} \tag{5.8}$$

The last step is to write both $a(r)$ and $\phi(r)$ in terms of (J,D) and (φ,θ) to write V_n in a form suitable to carry out the quasilinear analysis. This requires finding a convenient basis to express $a(r)$ and $\phi(r)$. For quasilinear theory in an homogeneous plasma at rest, this basis is a Fourier set of plane waves associated with translation invariance. Within the framework of random phase approximation each Fourier component then acts separately in the quasilinear diffusion operator which is a sum over the square of the amplitude of these Fourier components.

In the case of interest the Fourier–Bessel expansion seems more natural given the cylindrical symmetry of the problem. An added motivation for this choice is that recent studies on the OAM Faraday–Fresnel effect (Rax & Gueroult 2021) have shown that the eigenmodes of the whistler branch in a rotating plasma are of the type described by (5.2) with in this case $a(r)$ the ordinary Bessel function $\mathrm{J}_n(kr)$, and that the eigenmodes of the Trievelpiece–Gould branch in a rotating plasma are of the type described by (5.1) with in this case $\phi(r)$ proportional to $\mathrm{J}_n(kr)$, with k fulfilling in each case an appropriate dispersion relation. Lastly, the Fourier–Bessel expansion theorem states that all the other branches of the plasma waves spectrum in a rotating plasma can similarly be written with waves of the type (5.1) and (5.2), and that $a(r)$ can be represented by $\tilde{a}(k)$ as the sum $a(r)=\int k\tilde{a}(k)\mathrm{J}_n(kr)\,\mathrm{d}k$ with $\tilde{a}(k)=\int ra(r)\mathrm{J}_n(kr)\,\mathrm{d}r$. Thus, without loss of generality, we consider transverse and longitudinal rotating and propagating cylindrical waves of the type

$$\boldsymbol{a}_{\pm}(\boldsymbol{r},t)=\mathrm{Re}\left[\frac{\mathcal{E}(\omega)}{j\omega}\mathrm{J}_n(kr)\exp j(n\alpha+\beta z-\omega t)\,\frac{\boldsymbol{e}_x\pm j\boldsymbol{e}_y}{\sqrt{2}}\right], \tag{5.9}$$

$$\phi(\boldsymbol{r},t)=\mathrm{Re}\left[\phi(\omega)\,\mathrm{J}_n(kr)\exp j(n\alpha+\beta z-\omega t)\right]. \tag{5.10}$$

Here $\mathcal{E}(\omega)$ and $\phi(\omega)$ are the spectral component of the transverse electric field and potential of a given cylindrical wave packet. The final quasilinear operator, quadratic in $\mathcal{E}$ and ϕ, will ultimately be summed over the full ω and $k(\omega)$ spectra. In this study though we do not specify the ω spectra and the $k(\omega,\beta,n)$ dispersion. To provide a general result we instead analyse the quasilinear dynamics under the influence of a single cylindrical component ((5.9) and (5.10)). The quasilinear effect of a wave packet is simply the sum over the effects of each Fourier–Bessel component as in the plane wave case.

In a homogeneous magnetized plasma at rest the Jacobi–Anger expansion is used to identify the harmonic cyclotron resonances of a plane wave. For the cylindrical waves

https://doi.org/10.1017/S0022377823000612 Published online by Cambridge University Press

described by (5.9) and (5.10) we instead consider the triangle ***OGC*** in figures 3 and 4 and apply Graf's addition theorem

$$\mathrm{J}_n\left(kr\right)\exp\left(jn\alpha\right)=\sum_{l=-\infty}^{l=+\infty}\mathrm{J}_{l+n}\left(k\sqrt{\frac{2D}{\Omega}}\right)\mathrm{J}_l\left(k\sqrt{\frac{2J}{\Omega}}\right)\exp j\left[\left(l+n\right)\theta+l\varphi\right]. \tag{5.11}$$

In the limit of zero Larmor radius the sum on the right-hand side reduces to the $l=0$ term only, whereas $l\neq 0$ terms capture FLR effects. One verifies that the larger k and the larger J/D, the more terms are needed to approach the left-hand side in (5.11). Plugging this result into (5.7) and (5.8), the Hamiltonian writes as

$$H=H_0\left(\boldsymbol{J}\right)+\mathrm{Re}\left[\sum_{l=-\infty}^{l=+\infty}V_{nl\sigma}\left(J,D\right)\exp j\left[\left(l+\sigma\right)\varphi+\left(l+n\right)\theta+\beta z-\omega t\right]\right], \tag{5.12}$$

where we introduced $\sigma\in[-1,0,+1]$ the SAM index such that the L, R and scalar wave perturbations $V_{nl\sigma}$ are given by

$$\begin{aligned}V_{n,l,\sigma=+1}=&\,\mathcal{E}\frac{\Omega_+}{\omega}\sqrt{\frac{J}{\Omega}}\mathrm{J}_{l+n}\left(k\sqrt{\frac{2D}{\Omega}}\right)\mathrm{J}_l\left(k\sqrt{\frac{2J}{\Omega}}\right)\\&-\mathcal{E}\frac{\Omega_-}{\omega}\sqrt{\frac{D}{\Omega}}\mathrm{J}_{l+1+n}\left(k\sqrt{\frac{2D}{\Omega}}\right)\mathrm{J}_{l+1}\left(k\sqrt{\frac{2J}{\Omega}}\right),\end{aligned} \tag{5.13}$$

$$\begin{aligned}V_{n,l,\sigma=-1}=&\,\mathcal{E}\frac{\Omega_-}{\omega}\sqrt{\frac{D}{\Omega}}\mathrm{J}_{l-1+n}\left(k\sqrt{\frac{2D}{\Omega}}\right)\mathrm{J}_{l-1}\left(k\sqrt{\frac{2J}{\Omega}}\right)\\&-\mathcal{E}\frac{\Omega_+}{\omega}\sqrt{\frac{J}{\Omega}}\mathrm{J}_{l+n}\left(k\sqrt{\frac{2D}{\Omega}}\right)\mathrm{J}_l\left(k\sqrt{\frac{2J}{\Omega}}\right),\end{aligned} \tag{5.14}$$

$$V_{n,l,\sigma=0}=\phi\mathrm{J}_{l+n}\left(k\sqrt{\frac{2D}{\Omega}}\right)\mathrm{J}_l\left(k\sqrt{\frac{2J}{\Omega}}\right). \tag{5.15}$$

In order to simplify the notation we define the vector

$$\boldsymbol{N}=\left[\left(l+\sigma\right),\left(l+n\right),\beta\right] \tag{5.16}$$

and use it as an index to specify n, l and σ. The Hamiltonian H in (5.7) then writes in compact form as

$$H\left(\boldsymbol{J},\boldsymbol{\theta},t\right)=H_0\left(\boldsymbol{J}\right)+\sum_N V_N\left(\boldsymbol{J}\right)\exp j\left(\boldsymbol{N}\cdot\boldsymbol{\theta}-\omega t\right), \tag{5.17}$$

where we dropped the Re mention for readability and $\sum_N=\sum_{l=-\infty}^{l=+\infty}$. This implies that both the OAM azimuthal number n of the cylindrical waves ((5.9) and (5.10)) and the SAM number σ remain fixed as we study separately L, R and potential waves.

For a purely rotating wave, characterized by n, σ and $\beta=0$, the structure of the relation (5.17) reveals a number of selection rules between the wave-induced small increments of

https://doi.org/10.1017/S0022377823000612 Published online by Cambridge University Press

actions and energy. These selection rules provide also the branching ratio between the exchange of the actions. To see this consider Hamilton's equations:

$$\frac{\mathrm{d}H}{\mathrm{d}t} = \frac{\partial H}{\partial t} = -j\omega \sum_N V_N(\boldsymbol{J}) \exp j(\boldsymbol{N}\cdot\boldsymbol{\theta} - \omega t), \tag{5.18}$$

$$\frac{\mathrm{d}L_C}{\mathrm{d}t} = \frac{\partial H}{\partial \varphi} - \frac{\partial H}{\partial \theta} = j(\sigma - n) \sum_N V_N(\boldsymbol{J}) \exp j(\boldsymbol{N}\cdot\boldsymbol{\theta} - \omega t). \tag{5.19}$$

A wave-induced small variation of the ion energy δH thus implies a small variation of the angular momentum δL_C through

$$\frac{\delta L_C}{\delta H} = \frac{n-\sigma}{\omega}. \tag{5.20}$$

Using $\delta H = \Omega_-\delta D - \Omega_+\delta J$ we can express the branching ration between the cyclotron kinetic energy channel and the potential energy channel as

$$\frac{\delta J}{\delta H} = \frac{l+\sigma}{\omega}, \tag{5.21}$$

$$\frac{\delta D}{\delta H} = \frac{l+n}{\omega}. \tag{5.22}$$

These relations provide a first basic tool to optimize phase space engineering. For example one may want to set up a radial current ($\delta D \neq 0$) but avoid ICRH heating ($\delta J = 0$). In this case, (5.21) and (5.22) point to waves such that $l + \sigma = 0$ but $l + n \neq 0$. However, the best strategy to optimize power deposition among the various energy channels is to consider the kinetic equation.

6. Brillouin resonances

6.1. *Resonance condition*

The Hamiltonian (5.17) makes it possible to identify the conditions for resonant coupling. For this we simply substitute the unperturbed motion $\boldsymbol{\theta} = \boldsymbol{\Omega} t + \boldsymbol{\theta}_0$ into the oscillating phase $j(\boldsymbol{N}\cdot\boldsymbol{\theta} - \omega t)$ of each $V_N \exp j(\boldsymbol{N}\cdot\boldsymbol{\theta} - \omega t)$ perturbation. We then obtain the phase factor $j(\boldsymbol{N}\cdot\boldsymbol{\Omega} - \omega)t + j\boldsymbol{\theta}_0$ which stops to rotate and becomes stationary when the resonance condition

$$\omega = \boldsymbol{N}\cdot\boldsymbol{\Omega} = -(l+\sigma)\,\Omega_+ + (l+n)\,\Omega_- + \beta P, \tag{6.1}$$

is fulfilled. This resonance condition replaces the classical Landau-cyclotron condition

$$\omega - \beta v_z = m\omega_c \tag{6.2}$$

with $m \in \mathbb{Z}$ and where v_z is the velocity along the magnetic field. Because this is the slow and fast Brillouin modes that are involved in (6.1) rather than the cyclotron frequency we call (6.1) the Brillouin resonance condition. One verifies as expected that (6.1) reduces to (6.2) when the static electric field (3.1) cancels. Rewriting (6.1) as

$$\omega - \beta P - (n+\sigma)\Omega_- = l(\omega_c + 2\Omega_-) + \sigma\omega_c, \tag{6.3}$$

the left-hand side is simply the Doppler-shifted wave frequency considering both the axial translation and the azimuthal rotation (Garetz 1981; Courtial *et al.* 1998). The first term on

https://doi.org/10.1017/S0022377823000612 Published online by Cambridge University Press

the right-hand side $l(\omega_c + 2\Omega_-)$ can then be interpreted as normal ($l > 0$) or anomalous ($l < 0$) Doppler effect modified by inertial effects. Indeed $\omega_c + 2\Omega_-$ is the gyrofrequency corrected by the Coriolis force for an ion rotating at the angular frequency Ω_-. The classical yet subtle picture of normal/anomalous Doppler effect can be extended to the cases where the helical motion of the guiding centre (P, Ω_-) is slower or faster than the axial (ω/β) and azimuthal (ω/n) phase velocities (Nezlin 1976).

At resonance $\exp j(\boldsymbol{N}\cdot\boldsymbol{\theta} - \omega)t = \exp j(\boldsymbol{N}\cdot\boldsymbol{\theta}_0)$. Some particles gain energy/momentum while others loose energy/momentum, with the sign of the variation determined by the phase factor $\mathrm{Re}(\exp j(\boldsymbol{N}\cdot\boldsymbol{\theta}_0))$. This diffusive behaviour of the actions is described within the framework of random phase approximation where we average over $\exp j(\boldsymbol{N}\cdot\boldsymbol{\theta}_0)$ the square of the action variations to construct the quasilinear diffusion equation. The construction of this kinetic description leading to the quasilinear equation can be done either through a Lagrangian or a Eulerian point of view in phase space (Rax 2021). Here we will use the latter, as reviewed in Appendix B.

Note finally that the resonance condition (6.1) can be recovered from a simple photon picture. For this we recall that a photon associated with a wave described by (2.1) carries an energy $\hbar\omega$ and a linear momentum along the z axis $\hbar\beta$. When this photon is absorbed by a rotating ion the variation of the particle energy H_0 and linear momentum P are given by

$$\delta H_0 = \hbar\omega, \quad \delta P = \hbar\beta. \tag{6.4}$$

Besides energy and axial linear momentum, the photon associated with the wave (2.1) also carries an OAM plus SAM angular momentum $(n \mp 1)\hbar$ along the z axis (see Appendix A). When this photon is absorbed by a rotating ion the change of the ion canonical angular momentum L_C is

$$\delta L_C = (n \mp 1)\,\hbar. \tag{6.5}$$

Equation (3.9) reveals the harmonic oscillators structure of the Hamiltonian H_0. We can thus draw an analogy with the Hamiltonian of the Landau levels of a magnetized quantum particle to conclude that, at the quantum level, the changes of the action J and D can only be an integer multiple of $\hbar$, that is

$$\delta J = n_J\hbar, \quad \delta D = n_D\hbar \tag{6.6a,b}$$

with $(n_J, n_D) \in \mathbb{Z}^2$ a pair of integers. In fact we are considering the quasiclassical limit with large quantum numbers: $n_J + 1/2 \sim n_J$ and $n_D + 1/2 \sim n_D$. Then, from (3.12) and (4.1), one finds

$$\delta L_C = \delta D - \delta J, \tag{6.7}$$

$$\delta H_0 = \Omega_-\delta D - \Omega_+\delta J + \delta P^2/2. \tag{6.8}$$

These two relations together with the semiclassical expansion $\delta P^2 = 2\hbar\beta P + O(\hbar^2)$ finally lead to

$$\omega - \beta P = -n_J\Omega_+ + (n_J + n \mp 1)\,\Omega_- + O(\hbar). \tag{6.9}$$

If $\hbar = 0$, we recognize a relation similar to our resonance condition identified in (6.1) with $n_J = l \pm 1$, supporting the simple photon picture.

https://doi.org/10.1017/S0022377823000612 Published online by Cambridge University Press

6.2. *Diffusion paths*

Besides the resonance lines (6.1), we can also identify from the Hamiltonian the diffusion paths along which resonant energy–momentum exchanges take place in actions space. Restricting the study to a single $V_N(\boldsymbol{J})$ resonant coupling in (5.17), Hamilton's equations near the resonance (6.1) write as

$$\left.\frac{\mathrm{d}\boldsymbol{J}}{\mathrm{d}t}\right|_{N\cdot\boldsymbol{\Omega}=\omega} = -jNV_N \exp jN\cdot\boldsymbol{\theta}_0, \tag{6.10}$$

$$\left.\frac{\mathrm{d}H}{\mathrm{d}t}\right|_{N\cdot\boldsymbol{\Omega}=\omega} = -j\omega V_N \exp jN\cdot\boldsymbol{\theta}_0. \tag{6.11}$$

Resonant actions variation (wave kicks) $\delta\boldsymbol{J}$ associated with a resonant energy variation δH are thus related by

$$\omega\delta\boldsymbol{J} = N\delta H. \tag{6.12}$$

Practically δH can be taken as δH_0 within the two time scales quasilinear framework reviewed in Appendix B. In fact, without invoking the ordering between the secular quasilinear evolution and the fast ω oscillation, we can simply evaluate a variation of H_0 in (3.12) and take into account (6.12) to obtain

$$\delta H_0 = \boldsymbol{\Omega}\cdot\delta\boldsymbol{J} = \boldsymbol{\Omega}\cdot N\frac{\delta H}{\omega} = \delta H \tag{6.13}$$

since $\omega = \boldsymbol{N}\cdot\boldsymbol{\Omega}$. Thus, the resonant wave kicks $\delta\boldsymbol{J}$ associated with a resonant energy exchange δH_0 between the rotating wave and the rotating particle are given by

$$[\delta J, \delta D, \delta P] = [(l+\sigma)\,,(l+n)\,,\beta]\,\frac{\delta H_0}{\omega} \tag{6.14}$$

for a given V_N coupling. In the weak field limit this reduces to

$$[\omega_c\rho_L\delta\rho_L, \omega_c R_g\delta R_g, \delta v_z] = [(l+\sigma)\,,(l+n)\,,\beta]\,\frac{\delta H_0}{M\omega}, \tag{6.15}$$

where we have temporarily reintroduced the ion mass M and the cyclotron frequency ω_c.

The relation (6.12) implies that there exists a linear combination of the actions which is invariant under the time evolution prescribed by the wave coupling $V_N \exp j(\boldsymbol{N}\cdot\boldsymbol{\theta} - \omega t)$, namely

$$\delta\,(\boldsymbol{N}\times\boldsymbol{J}) = 0. \tag{6.16}$$

Focusing on Brillouin resonances rather than on Landau resonances, we restrict the analysis to the case $\beta P = 0$. For a single V_N ((6.12) and (6.16)) then identify a diffusion path in action space (J, D). Specifically, the path passing through a resonant point (J_0, D_0) writes as

$$(l+n)\,(J-\mathrm{J}_0) = (l+\sigma)\,(D-D_0)\,. \tag{6.17}$$

This is illustrated in figure 5. The diffusion paths (6.17) are invariant under the dynamics driven by a single V_N coupling. Quasilinear diffusion in action space takes place along these diffusion paths provided that the resonant condition (6.1) is fulfilled and that $|V_{nl\sigma}(\mathrm{J}_0, D_0)|$ is not too small. Figure 5 also represents the isoenergy lines, i.e. points in

https://doi.org/10.1017/S0022377823000612 Published online by Cambridge University Press

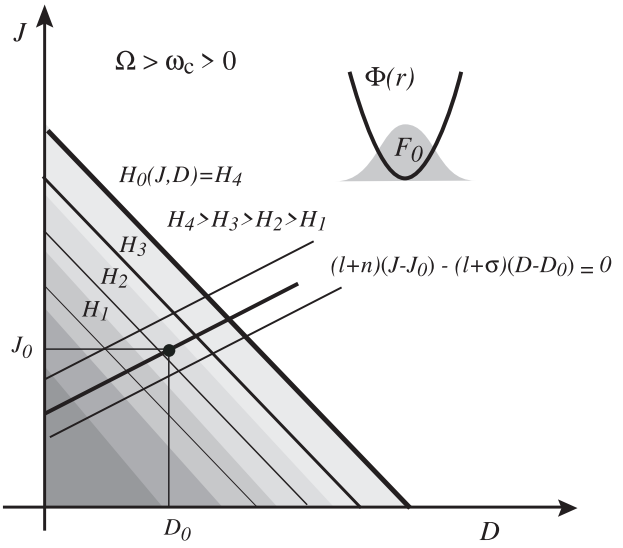

FIGURE 5. Isoenergy levels H_0 and diffusion paths in (J, D) action space.

(J, D) space where H_0 is constant. For $\Omega > \omega_c > 0$ the electric field is confining and we can consider a canonical equilibrium distribution function

$$F_0(\boldsymbol{J}) = \frac{\Omega^2 - \omega_c^2}{4\sqrt{2\pi}\,(k_B T)^{5/2}} \exp\left(-\frac{H_0(\boldsymbol{J})}{k_B T}\right), \tag{6.18}$$

where T is the temperature and we have taken the normalization $\int \mathrm{d}\boldsymbol{J} F_0 = 1$. The corresponding density levels in (J, D) space are colour coded in grey in figure 5. For $0 < \Omega \leq \omega_c$ the canonical distribution function (6.18) cannot be normalized as the potential $\phi(r)$ is not confining but instead either flat ($\Omega = \omega_c$) or hill shaped ($\Omega < \omega_c$).

6.3. *Small Larmor radius limit*

When the Larmor radius $\sqrt{2J/\Omega}$ is small compared with the radial wavelength $2\pi/k$, that is

$$k\sqrt{\frac{J}{2\Omega}} < 1, \tag{6.19}$$

the coupling coefficients $V_{n,l,\sigma}$ in (5.13), (5.14) and (5.15) can be simplified by using the small parameter expansion

$$\mathrm{J}_l\left(k\sqrt{\frac{J}{2\Omega}}\right) \sim \frac{\left(k\sqrt{\frac{J}{2\Omega}}\right)^l}{l!}. \tag{6.20}$$

We see that in this limit the $l = 0$ term is the most effective since it is associated with the largest $V_{n,l,\sigma}$. The resonance condition (6.1) for $l = 0$ then gives $\omega - \beta P = -\sigma\Omega_+ + n\Omega_-$ and the fundamental $l = 0$ Doppler-shifted cyclotron resonance term $\sigma\Omega_+$ is only due to the SAM content of the wave.

https://doi.org/10.1017/S0022377823000612 Published online by Cambridge University Press

If one assumes further $\sigma = 0$, as in the scalar case (5.10), and $\beta P = 0$, cyclotron and Landau terms are avoided and one gets get a pure OAM harmonic Brillouin–Landau resonance

$$\omega = n\Omega_- \tag{6.21}$$

between the drift rotation Ω_- and the wave OAM. This is the optimal choice for the sustainment of a plasma column rotation. The physical interpretation of (6.21) is simple: the wave angular velocity $\mathrm{d}\alpha/\mathrm{d}t = \omega/n$ is equal to the particle guiding centre angular velocity $-\mathrm{d}\theta/\mathrm{d}t = \Omega_-$.

6.4. *Special examples*

Let us illustrate the physics behind Brillouin coupling through three selected examples. Consider first a potential wave $\sigma = 0$, that is (5.10), with $\beta = 0$ and the small Larmor radius approximation such that $l = 0$. In these conditions $\boldsymbol{N} = [0, n, 0]$ and (6.14) writes as

$$\frac{\delta J}{\delta H_0} = 0, \quad \frac{\delta D}{\delta H_0} = \frac{1}{\Omega_-} \tag{6.22a,b}$$

since the Brillouin resonance (6.1) implies $\omega = n\Omega_-$. This result can be interpreted as follows. For absorption $\delta H_0 > 0$, the wave energy is transferred to potential energy through the wave-induced radial dynamics of the guiding centre in the electrostatic potential $\Phi(r)$. For emission $\delta H_0 < 0$, the potential energy of the particles is passed on to the wave energy. This type of instability is used for microwave generation in magnetrons. We note also that the simultaneous cooling ($\delta H_0 < 0$) and ash removal ($\delta D > 0$) of alpha particles in a rotating tokamak, through free energy extraction (Fisch & Rax 1992, 1993; Fisch & Herrmann 1994, 1995; Herrmann & Fisch 1997), is optimal in these wave conditions. The ratio of energy extraction to radial expulsion is then adjusted through Ω_-.

Consider now a vectorial wave $\sigma = \pm 1$, that is (5.9), with $\beta = 0$, no OAM ($n = 0$) and the small Larmor radius approximation such that $l = 0$. In these conditions $\boldsymbol{N} = [\sigma, 0, 0]$ and (6.14) writes as

$$\frac{\delta D}{\delta H_0} = 0, \quad \frac{\delta J}{\delta H_0} = -\frac{1}{\Omega_+} \tag{6.23a,b}$$

since the Brillouin resonance (6.1) implies $\omega = -\sigma\Omega_+$ (remember that $\Omega_+ < 0$). In this case the wave energy is simply passed into cyclotron energy $-\Omega_+\delta J$. This is the case of pure ICRH modified by inertial effects.

Consider finally a potential wave $\sigma = 0$, that is (5.10), with $\beta = 0$ and no OAM ($n = 0$), but with FLR effects $l \neq 0$. In these conditions $\boldsymbol{N} = [l, l, 0]$ and (6.12) writes as

$$\frac{\delta D}{\delta H_0} = \frac{1}{\Omega}, \quad \frac{\delta J}{\delta H_0} = \frac{1}{\Omega} \tag{6.24a,b}$$

since the Brillouin resonance (6.1) implies $\omega = -l\Omega_+ + l\Omega_- = l\Omega$. This result can be interpreted as follows. For absorption $\delta H_0 > 0$ the wave energy is transferred to both kinetic energy $-\Omega_+\delta J$ and potential energy $\Omega_-\delta D$ as shown by (3.12). The partitioning between these two energy channels must, however, fulfil conservation of canonical angular momentum $\delta L_C = 0$, which from (4.1) implies $\delta D = \delta J$. Conservation of L_C is indeed the consequence of the invariance through rotation of the Hamiltonian $H_0 + V$, since here the wave carries neither OAM ($n = 0$) nor SAM ($\sigma = 0$).

https://doi.org/10.1017/S0022377823000612 Published online by Cambridge University Press

7. Quasilinear theory in a rotating magnetized plasma

When a wave propagates in a plasma, two time scales are associated with the quasilinear ordering. One is the fast linear response that is described at the kinetic level by Vlasov's equation, whose solution gives the refractive/dispersive part of the dielectric tensor. The other is the slow, angle averaged, quasilinear evolution of the action distribution function $F(\boldsymbol{J}, t)$ which is described at the kinetic level by the quasilinear equation. The standard quasilinear equation (B10) is derived in Appendix B.

With the Hamiltonian (5.17), the evolution of the action distribution function $F(\boldsymbol{J}, t)$ in a magnetized rotating plasma is given by

$$\frac{\partial F}{\partial t} = \frac{\pi}{2} \sum_N \left(\boldsymbol{N} \cdot \frac{\partial}{\partial \boldsymbol{J}} \right) \left[|V_N|^2 \, \delta \left(\boldsymbol{N} \cdot \boldsymbol{\Omega} - \omega \right) \right] \left(\boldsymbol{N} \cdot \frac{\partial}{\partial \boldsymbol{J}} \right) F \left(\boldsymbol{J}, t \right), \tag{7.1}$$

where the V_N are those derived in (5.13), (5.14) and (5.15). The operator $\boldsymbol{N} \cdot \partial_J$ involved in this slow (with respect to $1/\omega$) diffusion in action space writes as

$$\boldsymbol{N} \cdot \frac{\partial}{\partial \boldsymbol{J}} = (l + \sigma) \, \frac{\partial}{\partial J} + (l + n) \, \frac{\partial}{\partial D} + \beta \frac{\partial}{\partial P}. \tag{7.2}$$

We normalize F by taking $\int \mathrm{d}\boldsymbol{J} F(\boldsymbol{J}, t) = 1$ and consider that $F(\boldsymbol{J} = +\infty, t) = 0$ and $F(J < 0, D < 0, P = -\infty, t) = 0$.

Introducing the resonant particles density ρ, the power per unit volume W lost or gained by the wave (and gained or lost by the plasma) is

$$\frac{W}{\rho} = \frac{\mathrm{d}}{\mathrm{d}t} \int \mathrm{d}\boldsymbol{J} H_0 \left(\boldsymbol{J} \right) F \left(\boldsymbol{J}, t \right) = \int \mathrm{d}\boldsymbol{J} H_0 \frac{\partial F}{\partial t} \tag{7.3}$$

where the integral is to be taken over $-\infty < J, D, P < +\infty$. Using (7.1) and integrating by parts the operator (7.2) gives

$$\frac{W}{\rho} = -\frac{\pi}{2} \int \mathrm{d}\boldsymbol{J} \omega \sum_N [|V_N|^2 \, \delta \left(\boldsymbol{N} \cdot \boldsymbol{\Omega} - \omega \right)] \boldsymbol{N} \cdot \frac{\partial F}{\partial \boldsymbol{J}}. \tag{7.4}$$

We recognize in (7.4) the power balance given by the dissipative part of the collisionless dielectric tensor. A second integration by parts then gives the density of power

$$W = \frac{\pi}{2} \rho \int \mathrm{d}\boldsymbol{J} F \left(\boldsymbol{J}, t \right) \omega \sum_N \boldsymbol{N} \cdot \frac{\partial}{\partial \boldsymbol{J}} [|V_N|^2 \, \delta \left(\boldsymbol{N} \cdot \boldsymbol{\Omega} - \omega \right)]. \tag{7.5}$$

Defining $w_N(\boldsymbol{J})$ through

$$W = \rho \sum_N \int \mathrm{d}\boldsymbol{J} F \left(\boldsymbol{J} \right) w_N \left(\boldsymbol{J} \right), \tag{7.6}$$

equation (7.5) then gives

$$w_N \left(\boldsymbol{J} \right) = \frac{\pi}{2} \omega \sum_N \boldsymbol{N} \cdot \frac{\partial}{\partial \boldsymbol{J}} [|V_N|^2 \, \delta \left(\boldsymbol{N} \cdot \boldsymbol{\Omega} - \omega \right)]. \tag{7.7}$$

This quantity is thus interpreted, for a single component V_N, as the power exchanged by a particle at $\boldsymbol{J}$ with this V_N component of the wave interaction. Equation (6.12) can hence

https://doi.org/10.1017/S0022377823000612 Published online by Cambridge University Press

be rewritten as

$$\left.\frac{\langle \delta \boldsymbol{J}\rangle}{\delta t}\right|_{N} = \frac{\boldsymbol{N}}{\omega}\frac{\delta H_0(\boldsymbol{J})}{\delta t} = \frac{\boldsymbol{N}}{\omega} w_N(\boldsymbol{J}), \tag{7.8}$$

where $\langle\ \rangle$ is an average over the fast phase of the wave and the $\boldsymbol{N}$ index restricts the wave kick $\delta\boldsymbol{J}$ to a single component V_N. Plugging (7.7) into (7.8) and using the tensorial product notation $\otimes$ yields

$$\frac{\langle \delta \boldsymbol{J}\rangle}{\delta t} = \frac{\pi}{2}\frac{\partial}{\partial \boldsymbol{J}} \cdot \sum_{N} \boldsymbol{N}\otimes\boldsymbol{N}\,|V_N|^2\,\delta(\boldsymbol{N}\cdot\boldsymbol{\Omega}-\omega). \tag{7.9}$$

This relation (7.9) is just the usual Einstein's relation (Fraiman & Kostyukov 1995) between the wave-induced drift coefficient $\langle\delta\boldsymbol{J}\rangle/\delta t$ and the wave-induced diffusion coefficient

$$\frac{\langle \delta\,\boldsymbol{J}\otimes\delta\boldsymbol{J}\rangle}{2\delta t} = \frac{\pi}{2}\sum_{N}\boldsymbol{N}\otimes\boldsymbol{N}[|V_N|^2\,\delta(\boldsymbol{N}\cdot\boldsymbol{\Omega}-\omega)] \tag{7.10}$$

used to write the kinetic equation (7.1) in the classical Fokker–Planck form with a drift and a diffusion coefficient

$$\frac{\partial F}{\partial t} = -\frac{\partial}{\partial \boldsymbol{J}}\cdot\left[\frac{\langle\delta\boldsymbol{J}\rangle}{\delta t}F - \frac{\partial}{\partial\boldsymbol{J}}\cdot\frac{\langle\delta\,\boldsymbol{J}\otimes\delta\boldsymbol{J}\rangle}{2\delta t}F\right] \tag{7.11}$$

rather than in the completely equivalent and more usual quasilinear form

$$\frac{\partial F}{\partial t} = \frac{\partial}{\partial \boldsymbol{J}}\cdot\left[\frac{\langle\delta\,\boldsymbol{J}\otimes\delta\boldsymbol{J}\rangle}{2\delta t}\cdot\frac{\partial F}{\partial\boldsymbol{J}}\right] \tag{7.12}$$

used here in (7.1). Einstein's relation

$$\frac{\langle\delta\boldsymbol{J}\rangle}{\delta t} = \partial_{\boldsymbol{J}}\cdot\frac{\langle\delta\,\boldsymbol{J}\otimes\delta\boldsymbol{J}\rangle}{2\delta t} \tag{7.13}$$

is a consequence of microreversibility (Rax 2021).

8. Angular momentum absorption

Short of solving the quasilinear equation (7.1), a clear understanding of the mechanism of angular momentum absorption (or emission) can be gained through the analysis of the quasilinear guiding centre radial velocity $\langle\delta D\rangle/\mathrm{d}t$ and quasilinear ICRH $\langle\delta J\rangle/\mathrm{d}t$ identified in (7.8) and (7.9). In general the effect of the wave is indeed two-fold: it both drives a radial drift current δD and provides ICRH δJ. Yet, this last channel should be avoided or at least minimized for fluid rotation sustainment. This can in principle be done through the choice of a suitable wave.

8.1. *Absorption from global angular momentum conservation*

For a single particle, the SAM (S_z) and OAM (L_z) lost by the wave during the resonant wave–particle interaction are gained by the particle in the form of canonical angular

https://doi.org/10.1017/S0022377823000612 Published online by Cambridge University Press

momentum L_C. From (4.1)

$$-\frac{\langle \delta L_C \rangle}{\delta t} = \frac{\langle \delta J \rangle}{\delta t} - \frac{\langle \delta D \rangle}{\delta t} \tag{8.1}$$

which using (7.9) rewrites as

$$-\frac{\langle \delta L_C \rangle}{\delta t} = (\sigma - n)\,\frac{\pi}{2}\sum_N \boldsymbol{N}\cdot\partial_{\boldsymbol{J}}[|V_N|^2\,\delta\,(\boldsymbol{N}\cdot\boldsymbol{\Omega} - \omega)]. \tag{8.2}$$

Under the simple photon picture developed at the end of § 6.1, global angular momentum conservation for the full system wave plus particle and a single $|V_N|$ coupling coefficient thus writes as

$$\delta\, L_z|_{\text{wave}} = -n\frac{\delta H_0}{\omega}, \quad \delta\, S_z|_{\text{wave}} = \sigma\frac{\delta H_0}{\omega}. \tag{8.3a,b}$$

Quasilinear theory brings additional insights in that it allows to relate the wave's change in angular momentum to the angular momentum absorption by a distribution function $F(\boldsymbol{J}, t)$. Specifically, averaging (8.2) over the distribution of actions in the plasma and integrating by parts gives

$$\left.\frac{\mathrm{d}\,(L_z + S_z)}{\mathrm{d}t}\right|_{\text{wave}} = (n-\sigma)\,\frac{\pi}{2}\iint \mathrm{d}J\,\mathrm{d}D\sum_l |V_N|^2\,\boldsymbol{N}\cdot\partial_{\boldsymbol{J}}\,F|_{P=P_l}\,. \tag{8.4}$$

Here P_l is the resonant axial momentum fulfilling the relation $\boldsymbol{N}\cdot\boldsymbol{\Omega} = \omega$ for given wave field and DC field configurations, that is

$$\beta P_l = \omega + (l+\sigma)\,\Omega_+ - (l+n)\,\Omega_-. \tag{8.5}$$

Note that since $-\infty < P < \infty$ there is always a solution P_l to (8.5) for a given $(l, n) \in \mathbb{Z}^2$. Note also that (8.4) can be equivalently derived from (8.3a,b) using (7.4).

The angular momentum absorption coefficient derived in (8.4) can be evaluated by considering the kinetic evolution of $F(\boldsymbol{J}, t)$ given in (7.1) together with a relaxation term associated with collisions. Assuming that the plasma equilibrium is only weakly perturbed by the wave we can consider that $F \sim F_0$ as given in (6.18).

8.2. *Physical picture*

To develop a deeper physical understanding of quasilinear angular momentum exchange we define the average kinetic angular momentum

$$\langle L_K \rangle = \langle x v_y - y v_x \rangle_{\theta+\varphi} = \frac{2\Omega_-}{\Omega} D + \frac{2\Omega_+}{\Omega} J \tag{8.6}$$

and the average magnetic flux through the orbit

$$\langle \Psi \rangle = \omega_c \pi \langle x^2 + y^2 \rangle_{\theta+\varphi} = 2\pi\frac{\omega_c}{\Omega} D + 2\pi\frac{\omega_c}{\Omega} J. \tag{8.7}$$

According to the quasilinear prescription, the bracket $\langle\rangle$ indicates an angle average of (3.14), (4.2) and (4.3). Meanwhile, (4.4) gives a relation for the canonical angular

https://doi.org/10.1017/S0022377823000612 Published online by Cambridge University Press

momentum variation

$$\delta L_C = \delta \langle L_K \rangle + \delta \langle \Psi \rangle / 2\pi. \tag{8.8}$$

From (8.6) and (8.7) the kinetic and magnetic components $\delta\langle L_K\rangle$ and $\delta\langle\Psi\rangle$ then write as

$$\Omega \delta \langle L_K \rangle = 2\Omega_- \delta D + 2\Omega_+ \delta J, \tag{8.9}$$

$$\Omega \delta \langle \Psi \rangle = 2\pi\omega_c \delta D + 2\pi\omega_c \delta J. \tag{8.10}$$

A physical interpretation of these results can be obtained as follows, where we focus again on the more intuitive ordering $D > J$.

Starting with the kinetic component (8.9), recall from § 4 that an ion with mass $M = 1$ displays a guiding centre moment of inertia $M_G = 2D/\Omega$ with respect to the z axis, and a moment of inertia of the cyclotron motion $M_C = 2J/\Omega$ with respect to the guiding centre. Recall also that the guiding centre of this ion rotates at $\mathrm{d}\theta/\mathrm{d}t = \Omega_-$ whereas the cyclotron rotation takes place at the angular frequency $\Omega_+ = -\mathrm{d}\varphi/\mathrm{d}t$. Now, because these two angular velocities are set by the fields ((3.1) and (3.2)), the variation of the kinetic angular momentum of the ion $\langle L_K\rangle = M_G\Omega_- + M_C\Omega_+$ (θ is anticlockwise and φ is clockwise) must come from a variation of the moments of inertia and not of the angular velocities, so that

$$\frac{\delta \langle L_K \rangle}{\delta t} = \frac{\delta M_G}{\delta t}\Omega_- + \frac{\delta M_C}{\delta t}\Omega_+ = \frac{2\Omega_-}{\Omega}\frac{\delta D}{\delta t} + \frac{2\Omega_+}{\Omega}\frac{\delta J}{\delta t}, \tag{8.11}$$

which is precisely (8.9).

The interpretation of the magnetic component

$$\frac{1}{2\pi}\frac{\delta \langle \Psi \rangle}{\delta t} = \frac{\omega_c}{\Omega}\frac{\delta D}{\delta t} + \frac{\omega_c}{\Omega}\frac{\delta J}{\delta t}, \tag{8.12}$$

requires an analysis of both the δD and δJ terms. As we will now show, these two terms can be interpreted in terms of two different torques exerted on an ion in the background magnetic field. Starting with D, two pictures can be invoked. The first one is to consider the axial torque due to the magnetic force exerted on a charge $q = 1$ moving radially. The radial velocity of this charge is

$$\frac{\mathrm{d}}{\mathrm{d}t}\left(\sqrt{\frac{2D}{\Omega}}\right)\boldsymbol{e}_r, \tag{8.13}$$

so that this torque writes as

$$\sqrt{\frac{2D}{\Omega}}\boldsymbol{e}_r \times \left[\frac{\mathrm{d}}{\mathrm{d}t}\left(\sqrt{\frac{2D}{\Omega}}\right)\boldsymbol{e}_r \times \omega_c \boldsymbol{e}_z\right] = -\frac{\omega_c}{\Omega}\frac{\mathrm{d}D}{\mathrm{d}t}\boldsymbol{e}_z. \tag{8.14}$$

The second is to consider an azimuthal electromotive force (emf) for a $q = 1$ charge distributed along a rotating circle with radius $\sqrt{2D/\Omega}$, associated with the variation of the loop surface as a result of the radial motion. This electric inductive field E_{emf} is also

https://doi.org/10.1017/S0022377823000612 Published online by Cambridge University Press

the source of an axial torque

$$\sqrt{\frac{2D}{\Omega}}\boldsymbol{e}_r \times E_{\rm emf}\boldsymbol{e}_\alpha = -\frac{1}{2\pi}\frac{{\rm d}\Psi_G}{{\rm d}t}\boldsymbol{e}_z = -\frac{\omega_c}{\Omega}\frac{{\rm d}D}{{\rm d}t}\boldsymbol{e}_z, \tag{8.15}$$

where we have introduced the magnetic flux through the guiding centre orbit Ψ_G and applied Faraday's law

$$-\frac{{\rm d}\Psi_G}{{\rm d}t} = \oint E_{\rm emf}\boldsymbol{e}_\alpha \cdot {\rm d}s\boldsymbol{e}_\alpha = 2\pi\sqrt{\frac{2D}{\Omega}}E_{\rm emf}. \tag{8.16}$$

One verifies that both analyses give the same axial torque experienced by an ion as a result of the wave-driven radial motion, which is precisely the first term on the right-hand side in (8.12). Moving on finally to the δJ term in (8.12), a similar current loop picture can be brought up but by considering a $q = 1$ charge distributed this time along the Larmor radius $\sqrt{2J/\Omega}$. The magnetic flux through this varying Larmor radius in indeed $\Psi_L = 2\pi(\omega_c/\Omega)J$, whose time derivative precisely gives back the second term on the right-hand side in (8.12)

In summary, the first term on the right-hand side of (8.8) corresponds to a change of the moment of inertia of the particle as a result of the quasilinear radial drift and Larmor radius evolution. The second term on the right-hand side of (8.8) corresponds to torques which result from a change in magnetic fluxes. Both of these terms, interpreted here in the weak field limit, must be balanced by the transfer of a corresponding angular momentum from the wave. Note, however, that the wave quasilinear primary effect is not a torque, it is a wave-driven radial current.

9. Radial current generation

Two types of model can be constructed from the quasilinear kinetic equation derived in (7.1). One option is to balance the quasilinear evolution of the distribution function with a collisional evolution at the kinetic level and then to average the solution $F(\boldsymbol{J})$ to obtain a steady state fluid picture. The other is to average the quasilinear dynamics to derive the fluid quasilinear flows of mass, charge and momentum, and then to balance these fluid flows with the dissipative terms involved in classical transport theory. The latter option is used in the following, where we further assume for simplicity axial homogeneity along z.

Let us write

$$\boldsymbol{\Gamma}\,(r) = \Gamma_r\boldsymbol{e}_r + \Gamma_\alpha\boldsymbol{e}_\alpha + \Gamma_z\boldsymbol{e}_z \tag{9.1}$$

the wave-driven particle flux which results from the absorption of the wave power $w_N(r)$ at radius r. The radial flow Γ_r is due to the wave-driven guiding centre radial velocity, which we showed is proportional to $\langle\delta D\rangle/\delta t$. The azimuthal flow Γ_α is a small diamagnetic effect associated with inhomogeneous wave-driven ICRH proportional to $\langle\delta J\rangle/\delta t$. The axial flow Γ_z is simply the wave-driven current from classical current generation (Fisch 1978, 1987) due to $\langle\delta P\rangle/\delta t$. The amplitude of these fluxes is governed by the evolution equation (7.8).

An analytical expression for the radial flow Γ_r can be derived if focusing once again on the familiar limit $J < D$. In this limit the average radial position of a resonant particle is $r^2 = 2D/\Omega$, and the average Lagrangian radial velocity is hence $r\Omega\,{\rm d}r/{\rm d}t = {\rm d}D/{\rm d}t$. From (7.8) the phase averaged evolution of D is proportional to the absorbed power w_N associated with the l harmonic Brillouin resonance for a rotating wave with azimuthal

https://doi.org/10.1017/S0022377823000612 Published online by Cambridge University Press

number n, and one has

$$\left.\frac{\langle \delta D \rangle}{\delta t}\right|_N = \frac{l+n}{\omega}\, w_N|_{D=\Omega r^2/2}. \tag{9.2}$$

Introducing back the particle mass M, and using the power density absorbed by the plasma W_N (in W m^{-3}) rather than w_N (in Watt), the wave-driven resonant particle flux is

$$\Gamma_r = \frac{(l+n)}{rM\Omega\omega} W_N \quad \mathrm{s}^{-1}\,\mathrm{m}^{-2}. \tag{9.3}$$

Consider now that the wave power density $W_N(t)$ is turned on adiabatically at $t=-\infty$ with $W_N(-\infty)=0$. The wave moves some resonant particles across the magnetic field, which leads to a radial current $\mathrm{J}_W(t)$ such that $\mathrm{J}_W(t=-\infty)=0$ and $\mathrm{J}_W(t=0)=q\Gamma_r$. The resulting time evolution of the radial electric field can be described as follows. From an electrical point of view, the build-up corresponds to a capacitive electric field build-up in a dielectric media, akin to the charging of a cylindrical capacitor. By considering the plasma as a dielectric with low frequency permittivity

$$\varepsilon = 1 + \left(\frac{\omega_{pi}}{\omega}\right)^2 \approx \left(\frac{\omega_{pi}}{\omega}\right)^2 \tag{9.4}$$

with ω_{pi} the ion plasma frequency, the electric field $\boldsymbol{E}(t)$ throughout this transient phase is thus determined from Maxwell–Ampère equation

$$\varepsilon_0 \frac{\omega_{pi}^2}{\omega_{ci}^2} \frac{\partial \boldsymbol{E}}{\partial t} + \mathrm{J}_W(t)\, \boldsymbol{e}_r = \boldsymbol{0}. \tag{9.5}$$

From a mechanical point of view this build-up phase corresponds to an angular momentum input via the $\mathrm{J}_W(t)\boldsymbol{e}_r \times \boldsymbol{B}$ force, and this momentum is converted into plasma $E \times B$ drift. Indeed, integrating (9.5) over the transient phase gives

$$\int_{-\infty}^{0} \mathrm{J}_W(t)\, \boldsymbol{e}_r \times \boldsymbol{B}\, \mathrm{d}t = -N_p M \frac{\boldsymbol{E}_0 \times \boldsymbol{B}}{B^2} \tag{9.6}$$

with $\boldsymbol{E}_0 = \boldsymbol{E}(t=0)$, M the ion mass and N_p the ion density, which confirms this momentum balance. Note that ion diamagnetic effects have been neglected in writing (9.5). Note also that because the conductivity along magnetic field lines is generally far larger than the conductivity across the field lines, charges rapidly move away from the wave active regions along the field lines, which in turn become equipotential.

Finally, for $t>0$, the charge separation induced by the wave is short circuited by the plasma perpendicular conductivity (Helander & Sigmar 2005; Kolmes *et al.* 2019; Rax *et al.* 2019). In this steady-state dissipative regime the wave-driven current $q\Gamma_r \boldsymbol{e}_r$ is balanced by a weak discharging Ohmic current $\boldsymbol{J}_{\mathrm{conduction}}$, with

$$\boldsymbol{\nabla} \cdot [q\Gamma_r \boldsymbol{e}_r + \boldsymbol{J}_{\mathrm{conduction}}] = 0. \tag{9.7}$$

Thus, as opposed to axial current generation, the steady-state is determined by the geometry of the plasma. The examination of this problem is left for a future study.

https://doi.org/10.1017/S0022377823000612 Published online by Cambridge University Press

10. Conclusions

Although angular momentum exchange between a wave and a rotating plasma is of importance both to astrophysics (Goldreich & Julian 1969; Julian 1973; Ferrière 2006) and laboratory plasmas (Kostyukov *et al.* 2002; Shvets, Fisch & Rax 2002; Thaury *et al.* 2013), a kinetic model of this interaction had to our knowledge never been proposed. In this study we addressed this issue and derived the quasilinear equation describing the interaction between a rotating wave and a rotating magnetized plasma. We further used this kinetic model to analyse angular momentum absorption/emission and to understand the interplay between OAM, SAM and FLR effects.

First, a canonical angle–action Hamiltonian description of the unperturbed Brillouin rotation dynamics in a rotating plasma is derived. The identification of angle–action variables allows to separate the fast part of the unperturbed motion (angles) from the constant (integrable system) or slow (adiabatic system) part of the unperturbed motion (actions). Through this process we identify three canonical actions D, J and P. The latter is the classical momentum along $\boldsymbol{B}$. The first two D and J are shown in the weak field limit, that is, for a cross-field drift frequency $E/(rB)$ small compared with the ion gyrofrequency, to be related to the magnetic flux through the cyclotron orbit and the guiding centre orbit.

Then, the wave–particle coupling is expressed in terms of these angle–action variables in the form of a perturbed Hamiltonian. This approach made it possible to identify a new resonance condition, which generalizes the classical Landau-cyclotron resonance to the case of a rotating plasma interacting with a rotating wave. This new condition, (6.1), is referred to as Brillouin resonance. It notably expresses FLR effects through (5.13) and (5.14), (5.15), which are found to be responsible for the occurrence of harmonic (l) Brillouin resonances. Together with this resonance condition, diffusion paths in action space were identified, and particular examples were exposed in the weak field limit. Finally, the quasilinear equation (7.1) which describes energy–momentum exchange as a time evolution of the actions distribution function was derived by averaging the kinetic response of the plasma to the perturbation over the fast part of the motion (angles).

By analysing the variation in canonical actions D and J predicted by the quasilinear equation, a physical picture for momentum absorption was finally proposed. Specifically, angular momentum from the wave was shown to be transferred to the plasma either as a change of the inertia tensor of the plasma, or as a magnetic flux variation ((8.11) and (8.12)). This analysis also showed that the radial flux can be identified as the source of angular momentum injection in the plasma. An interesting prospect is the generalization of this work to magnetic field inhomogeneities. The use of action-angle coordinates for the motion in a straight magnetic field with constant gradient (Brizard 2022) may for instance enable to capture bounce resonances in a mirror geometry rather than the uniform z translation Doppler shift considered here.

Finally, since the radial current is proportional to the absorbed power, sustaining steady-state rotation with waves will require adjusting the wave power deposition profile in a way that (9.7) is fulfilled. The optimization of power deposition will be the object of future studies, but we note for example that for a resonance $\boldsymbol{N}$ in a rotating magnetized plasma cylinder with large conductivity along the field lines $\eta_{\shortparallel}$ and weak conductivity across the field lines $\eta_{\perp}$, (9.7) gives

$$W_N(r) \approx \eta_{\perp} \frac{M^2}{q^2} \frac{\Omega\omega}{(l+n)} \left(\frac{\omega_c^2 - \Omega^2}{4} \right) r^2. \tag{10.1}$$

How this power density can be deposited in the plasma requires information on what the normal modes of a rotating plasma column are, and in particular the dispersion relation

https://doi.org/10.1017/S0022377823000612 Published online by Cambridge University Press

characterizing these modes, beyond the simple case of an aligned rotator (Gueroult *et al.* 2019*b*, 2020; Gueroult, Rax & Fisch 2023). This important question will be addressed in forthcoming studies.

Acknowledgements

The authors would like to thank Dr I.E. Ochs, E.J. Kolmes, T. Rubin and M.E. Mlodik for constructive discussions.

Editor Thierry Passot thanks the referees for their advice in evaluating this article.

Funding

This work was supported by the US Department of Energy (N.J.F., grant numbers DOE DE-SC0016072, NNSA DE-SC0021248); and the French National Research Agency (R.G., grant number ANR-21-CE30-0002). J.-M.R. acknowledges Princeton University and the Andlinger Center for Energy and the Environment for the ACEE fellowship which made this work possible.

Declaration of interests

The authors report no conflict of interest.

Appendix A. The SAM and OAM of a vector field

Consider a wave field $\boldsymbol{A}(\boldsymbol{r})\exp j\omega t$. The identification of (i) linear momentum, (ii) SAM and (iii) OAM eigenstates can be guided by the analysis of the transformation properties of the wave under translations and rotations.

For this consider first the change of this vector field $\boldsymbol{A}(\boldsymbol{r})$ under an active (change of the object $\boldsymbol{A}$), or a passive (change of the frame and coordinates used to describe $\boldsymbol{A}$), infinitesimal translation $\hat{T}$ associated with the small vector $\delta\boldsymbol{r}$:

$$\hat{T}\boldsymbol{A}\,(\boldsymbol{r}) = \boldsymbol{A}\,(\boldsymbol{r} \pm \delta\boldsymbol{r}) = \boldsymbol{A}\,(\boldsymbol{r}) \pm \delta\boldsymbol{r}\cdot\nabla\boldsymbol{A}\,(\boldsymbol{r})\,. \tag{A1}$$

The minus or plus signs are associated with the passive or the active points of view. Equation (A1) can be rewritten as a near identity transformation

$$\hat{T}\boldsymbol{A}\,(\boldsymbol{r}) = [\boldsymbol{I} \pm j\delta\boldsymbol{r}\cdot\hat{\boldsymbol{P}}]\boldsymbol{A}\,(\boldsymbol{r})\,, \tag{A2}$$

where $\boldsymbol{I}$ is the identity operator. The linear momentum operator $\hat{\boldsymbol{P}}$ is defined in the usual way as $\hat{\boldsymbol{P}} = -j\nabla$. The eigenvectors of this linear momentum operator $\hat{\boldsymbol{P}}$ are the plane waves, $\widehat{P}_z(\exp j\beta z) = \beta(\exp j\beta z)$, which are also solutions of Maxwell–Ampère and Maxwell–Faraday equations in a homogeneous linear dispersive plasma provided that $\beta(\omega)$ fulfils the dispersion relation.

Consider now the change of a vector field $\boldsymbol{A}(\boldsymbol{r})$ under an active, or a passive, infinitesimal rotation $\hat{R}$ associated with a small $\delta\alpha$ turn around an axis directed by a given unit vector $\boldsymbol{n}$ ($\boldsymbol{n}^2 = 1$):

$$\begin{aligned}\hat{R}\boldsymbol{A}\,(\boldsymbol{r}) &= \boldsymbol{A}\,(\boldsymbol{r} \pm \delta\alpha\boldsymbol{n}\times\boldsymbol{r}) \pm \delta\alpha\boldsymbol{n}\times\boldsymbol{A}\,(\boldsymbol{r} \pm \delta\alpha\boldsymbol{n}\times\boldsymbol{r})\\ &= \boldsymbol{A}\,(\boldsymbol{r}) \pm \delta\alpha\,[\boldsymbol{n}\times + (\boldsymbol{n}\times\boldsymbol{r})\cdot\nabla]\,\boldsymbol{A}\,(\boldsymbol{r})\,.\end{aligned} \tag{A3}$$

Equation (A3) can be rewritten as a near identity transformation displaying the separation between OAM and SAM operators

$$\hat{R}\boldsymbol{A}\,(\boldsymbol{r}) = [\boldsymbol{I} \pm j\delta\alpha\boldsymbol{n}\cdot(\hat{\boldsymbol{L}} + \hat{\boldsymbol{S}})]\boldsymbol{A}(\boldsymbol{r}). \tag{A4}$$

https://doi.org/10.1017/S0022377823000612 Published online by Cambridge University Press

The OAM operator $\hat{\boldsymbol{L}}$ and the SAM operator $\hat{\boldsymbol{S}}$ are thus defined according to the usual relations

$$\hat{\boldsymbol{L}} = -j\boldsymbol{r} \times \boldsymbol{\nabla}, \tag{A5}$$

$$\hat{\boldsymbol{S}} = -j\boldsymbol{n} \times . \tag{A6}$$

Note that, since $\hat{S}_x^2 + \hat{S}_y^2 + \hat{S}_z^2 = 2\boldsymbol{I}$, we recover the usual angular momentum rule for a vector: $\hat{\boldsymbol{S}}^2 = s(s+1)\boldsymbol{I}$ with $s = 1$.

We now restrict the transformations to rotations around the magnetic field direction in which case the angular momentum operator reduces to its z component $\hat{L}_z + \hat{S}_z$. The eigenvectors of the (i) OAM operator $\hat{L}_z$ and of the (ii) SAM operator $\hat{S}_z$ are (i) $\exp \pm jn\alpha$, where α is the polar angle around the magnetic field, and (iii) the L and R circularly polarized waves basis with eigenvalues ± 1 and $\boldsymbol{e}_z$ with zero eigenvalue

$$(\hat{L}_z + \hat{S}_z)\left(\frac{\boldsymbol{e}_x \pm j\boldsymbol{e}_y}{\sqrt{2}} \exp jn\alpha\right) = (n \mp 1)\left(\frac{\boldsymbol{e}_x \pm j\boldsymbol{e}_y}{\sqrt{2}} \exp jn\alpha\right). \tag{A7}$$

Solutions of Maxwell–Ampère and Maxwell–Faraday equations with a factor $\exp \pm jn\alpha$ have a well-defined OAM in rotating magnetized plasma when the magnetic axis is also the rotation axis. Solution of Maxwell–Ampère and Maxwell–Faraday equations with a polarization $\boldsymbol{e}_x \pm j\boldsymbol{e}_y$ have a well-defined SAM.

Appendix B. Canonical quasilinear equation

In this appendix we briefly review the derivation of the canonical quasilinear equation (Rax 2021).

Consider an integrable Hamiltonian H_0 (the adiabatic trap) and an oscillating perturbation (the wave) such that $V \ll H_0$. The kinetic description of wave particle interaction can be performed through a two time scales separation: $F(\boldsymbol{J}, t)$ is the distribution function in action space describing the slow evolution ($\partial_t F(\boldsymbol{J}, t) \sim O(V^2)$) of a given population and $f(\boldsymbol{J}, \boldsymbol{\theta}, t) \sim O(V)$ describes the fast-oscillating evolution ($\partial_t f(\boldsymbol{J}, \boldsymbol{\theta}, t) \sim O(V)$) in phase space

$$\mathcal{H} = H_0(\boldsymbol{J}) + V(\boldsymbol{J}, \boldsymbol{\theta}, t), \tag{B1}$$

$$\mathcal{F} = F(\boldsymbol{J}, t) + f(\boldsymbol{J}, \boldsymbol{\theta}, t). \tag{B2}$$

Here $(\boldsymbol{J}, \boldsymbol{\theta})$ is a set of action-angle variables for the unperturbed dynamics, $\boldsymbol{\Omega} = \partial H_0/\partial \boldsymbol{J}$, $\mathcal{H}$ is the perturbed Hamiltonian and $\mathcal{F}$ is the distribution function providing a kinetic description of the perturbed dynamics. Liouville's equation can be written with the help of Poisson bracket as $\partial_t \mathcal{F} = \{\mathcal{H}, \mathcal{F}\}$

$$\frac{\partial}{\partial t}(F + f) = \{(H_0 + V), (F + f)\}. \tag{B3}$$

Because $\{H_0, F\} = 0$ we can split this relation into (i) an $O(V)$ fast evolution – the Vlasov equation (B4) – and (ii) an $O(V^2)$ slow secular evolution – the quasilinear equation (B5) – ,

https://doi.org/10.1017/S0022377823000612 Published online by Cambridge University Press

so that

$$\frac{\partial f}{\partial t} = \{V, F\} + \{H_0, f\} \sim O(V), \tag{B4}$$

$$\frac{\partial F}{\partial t} = \langle \{V, f\} \rangle_{\boldsymbol{\theta}} \sim O\left(V^2\right), \tag{B5}$$

where we write $\langle\rangle_{\boldsymbol{\theta}}$ the average over the fast rotating angles $\boldsymbol{\theta}$.

The next step is to consider a Fourier decomposition of the $O(V)$ oscillating Vlasov terms. This decomposition is always possible as f and V are periodic functions of the angle $\boldsymbol{\theta}$, through the derivation of the Fourier coefficient often requires some lengthy calculations

$$V(\boldsymbol{J}, \boldsymbol{\theta}, t) = \sum_N V_N(\boldsymbol{J}) \exp j(\boldsymbol{N} \cdot \boldsymbol{\theta} - \omega t), \tag{B6}$$

$$f(\boldsymbol{J}, \boldsymbol{\theta}, t) = \sum_N f_N(\boldsymbol{J}) \exp j(\boldsymbol{N} \cdot \boldsymbol{\theta} - \omega t), \tag{B7}$$

where $N \in \mathbb{Z}^3$. With this Fourier decomposition Vlasov's equation Equation (B4) becomes an algebraic equation whose solution is

$$f = \sum_N \frac{V_N(\boldsymbol{J})}{\boldsymbol{N} \cdot \boldsymbol{\Omega} - \omega} \boldsymbol{N} \cdot \frac{\partial F}{\partial \boldsymbol{J}} + j\pi \sum_{\boldsymbol{n}} V_N(\boldsymbol{J}) \delta(\boldsymbol{N} \cdot \boldsymbol{\Omega} - \omega) \boldsymbol{N} \cdot \frac{\partial F}{\partial \boldsymbol{J}}. \tag{B8}$$

We recognize the adiabatic part of the plasma response, which ultimately provides the Hermitian part of the dielectric tensor, and the resonant part which provides the description of collisionless dissipation. In order to average (B5)

$$\frac{\partial F}{\partial t} = \left\langle \frac{\partial V}{\partial \boldsymbol{\theta}} \cdot \frac{\partial f}{\partial \boldsymbol{J}} - \frac{\partial f}{\partial \boldsymbol{\theta}} \cdot \frac{\partial V}{\partial \boldsymbol{J}} \right\rangle_{\boldsymbol{\theta}} \tag{B9}$$

we use the usual rule $\langle \mathrm{Re}[a(u)]\mathrm{Re}[b(u)] \rangle_u = \mathrm{Re}[a(u)b^*(u)]/2$ and finally obtain the canonical form

$$\frac{\partial F}{\partial t} = \partial_J \cdot \sum_N \boldsymbol{N} \mathrm{Re}\left(j \frac{V_N f_N^*}{2}\right) = \frac{\pi}{2} \frac{\partial}{\partial \boldsymbol{J}} \cdot \left[\sum_N \boldsymbol{N} |V_N|^2 \delta(\boldsymbol{N} \cdot \boldsymbol{\Omega} - \omega) \boldsymbol{N} \cdot \frac{\partial F}{\partial \boldsymbol{J}} \right], \tag{B10}$$

used in (7.1).

REFERENCES

Barber, P.B., Swift, D.A. & Tozer, B.A. 1972 The formation of rotating plasmas in a homopolar configuration. *J. Phys. D: Appl. Phys.* **5** (4), 693.

Barnett, S.M. & Allen, L. 1994 Orbital angular momentum and nonparaxial light beams. *Opt. Commun.* **110** (5–6), 670–678.

Barnett, S.M., Babiker, M. & Padgett, M.J. 2017 Optical orbital angular momentum. *Phil. Trans. R. Soc.* A **375** (2087), 20150444.

Bekhtenev, A.A., Volosov, V.I., Pal'chikov, V.E., Pekker, M.S. & Yudin, Y.N. 1980 Problems of a thermonuclear reactor with a rotating plasma. *Nucl. Fusion* **20** (5), 579–598.

Bliokh, K.Y. & Bliokh, Y.P. 2022 Momentum, angular momentum, and spin of waves in an isotropic collisionless plasma. *Phys. Rev.* E **105** (6), 065208.

https://doi.org/10.1017/S0022377823000612 Published online by Cambridge University Press

BONNEVIER, B. 1966 Diffusion due to ion–ion collisions in a multicomponent plasma. *Ark. Fys.* **33**, 255.

BRILLOUIN, L. 1945 A theorem of Larmor and its importance for electrons in magnetic fields. *Phys. Rev.* **67** (7–8), 260–266.

BRIZARD, A.J. 2022 Action–angle coordinates for motion in a straight magnetic field with constant gradient. *Commun. Nonlinear Sci. Numer. Simul.* **114**, 106652.

CHEN, F.F. 1984 *Introduction to Plasma Physics and Controlled Fusion*, 2nd edn. Springer.

CHEN, Q., QIN, H. & LIU, J. 2017 Photons, phonons, and plasmons with orbital angular momentum in plasmas. *Sci. Rep.* **7** (1), 41731.

COURTIAL, J., ROBERTSON, D.A., DHOLAKIA, K., ALLEN, L. & PADGETT, M.J. 1998 Rotational frequency shift of a light beam. *Phys. Rev. Lett.* **81** (22), 4828–4830.

DAVIDSON, R.C. 2001 *Physics of Nonneutral Plasmas*. Imperial College Press.

DAVIDSON, R.C. & KRALL, N.A. 1969 Vlasov description of an electron gas in a magnetic field. *Phys. Rev. Lett.* **22** (16), 833–837.

DODIN, I.Y. 2022 Quasilinear theory for inhomogeneous plasma. *J. Plasma Phys.* **88** (4), 905880407.

DOLGOLENKO, D.A. & MUROMKIN, Y.A. 2017 Separation of mixtures of chemical elements in plasma. *Phys. Uspekhi* **60** (10), 994.

EGGLESTON, D.L. & O'NEIL, T.M. 1999 Theory of asymmetry-induced transport in a non-neutral plasma. *Phys. Plasmas* **6** (7), 2699–2704.

VAN ENK, S.J. & NIENHUIS, G. 1994 Spin and orbital angular momentum of photons. *Europhys. Lett.* **25** (7), 497–501.

FERRIÈRE, K.M. 2006 Magnetospheric ULF waves: synthesis and new directions. In *Waves and Instabilities in a Rotating Environment*, Geophysical Monograph Series, (ed. K. Takahashi, P.J. Chi & R.L. Lysak), vol. 169, p. 157. Wiley.

FETTERMAN, A.J. & FISCH, N.J. 2008 Alpha channeling in a rotating plasma. *Phys. Rev. Lett.* **101** (20), 205003.

FETTERMAN, A.J. & FISCH, N.J. 2010 Alpha channeling in rotating plasma with stationary waves. *Phys. Plasmas* **17** (4), 042112.

FISCH, N. & HERRMANN, M. 1994 Utility of extracting alpha particle energy by waves. *Nucl. Fusion* **34** (12), 1541–1556.

FISCH, N. & HERRMANN, M. 1995 Alpha power channelling with two waves. *Nucl. Fusion* **35** (12), 1753–1760.

FISCH, N.J. 1978 Confining a tokamak plasma with rf-driven currents. *Phys. Rev. Lett.* **41** (13), 873–876.

FISCH, N.J. 1987 Theory of current drive in plasmas. *Rev. Mod. Phys.* **59** (1), 175–234.

FISCH, N.J. & RAX, J.-M. 1992 Interaction of energetic alpha particles with intense lower hybrid waves. *Phys. Rev. Lett.* **69** (4), 612–615.

FISCH, N.J. & RAX, J.-M. 1993 Free energy in plasmas under wave-induced diffusion. *Phys. Fluids* B **5** (6), 1754–1759.

FRAIMAN, G.M. & KOSTYUKOV, I.Y. 1995 Influence of external inhomogeneous static fields on interaction between beam of charged particles and packet of electromagnetic waves. *Phys. Plasmas* **2** (3), 923–934.

GARETZ, B.A. 1981 Angular Doppler effect. *J. Opt. Soc. Am.* **71** (5), 609.

GOLDREICH, P. & JULIAN, W.H. 1969 Pulsar electrodynamics. *Astrophys. J.* **157**, 869.

GÖTTE, J.B., BARNETT, S.M. & PADGETT, M. 2007 On the dragging of light by a rotating medium. *Proc. R. Soc.* A **463** (2085), 2185.

GOUGH, W. 1986 The angular momentum of radiation. *Eur. J. Phys.* **7** (2), 81–87.

GUEROULT, R. & FISCH, N.J. 2014 Plasma mass filtering for separation of actinides from lanthanides. *Plasma Sources Sci. Technol.* **23** (3), 035002.

GUEROULT, R., HOBBS, D.T. & FISCH, N.J. 2015 Plasma filtering techniques for nuclear waste remediation. *J. Hazard. Mater.* **297**, 153–159.

GUEROULT, R., RAX, J.-M. & FISCH, N.J. 2019a A necessary condition for perpendicular electric field control in magnetized plasmas. *Phys. Plasmas* **26** (12), 122106.

GUEROULT, R., RAX, J.-M. & FISCH, N.J. 2020 Enhanced tuneable rotatory power in a rotating plasma. *Phys. Rev.* E **102** (5), 051202(R).

GUEROULT, R., RAX, J.-M. & FISCH, N.J. 2023 Wave propagation in rotating magnetised plasmas. *Plasma Phys. Control. Fusion* **65** (3), 034006.

GUEROULT, R., RAX, J.M. & FISCH, N.J. 2018 Opportunities for plasma separation techniques in rare earth elements recycling. *J. Clean. Prod.* **182**, 1060–1069.

GUEROULT, R., SHI, Y., RAX, J.-M. & FISCH, N.J. 2019b Determining the rotation direction in pulsars. *Nat. Commun.* **10** (1), 3232.

GUEROULT, R., ZWEBEN, S.J., FISCH, N.J. & RAX, J.-M. 2019c E $\times$ b configurations for high-throughput plasma mass separation: an outlook on possibilities and challenges. *Phys. Plasmas* **26** (4), 043511.

HASSAM, A.B. 1997 Steady-state centrifugally confined plasmas for fusion. *Comments Plasma Phys. Control. Fusion* **18**, 263.

HELANDER, P. & SIGMAR, D.J. 2005 *Collisional Transport in Magnetized Plasmas*. Cambridge University Press.

HERRMANN, M.C. & FISCH, N.J. 1997 Cooling energetic particles in a tokamak with waves. *Phys. Rev. Lett.* **79** (8), 1495–1498.

JANES, G.S. 1965 Experiments on magnetically produced and confined electron clouds. *Phys. Rev. Lett.* **15** (4), 135–138.

JANES, G.S., LEVY, R.H., BETHE, H.A. & FELD, B.T. 1966 New type of accelerator for heavy ions. *Phys. Rev.* **145** (3), 925–952.

JANES, G.S., LEVY, R.H. & PETSCHEK, H.E. 1965 Production of BeV potential wells. *Phys. Rev. Lett.* **15** (4), 138–140.

JONES, R.V. 1976 Rotary aether drag. *Proc. R. Soc.* A **349** (1659), 423–439.

JULIAN, W.H. 1973 Pulsar electrodynamics. II. *Astrophys. J.* **183**, 967.

KAUFMAN, A.N. 1971 Resonant interactions between particles and normal modes in a cylindrical plasma. *Phys. Fluids* **14** (2), 387.

KIWAMOTO, Y., SOGA, Y. & AOKI, J. 2005 Radial transport in magnetized non-neutral plasma driven by rotating wave. *Phys. Plasmas* **12** (9), 094501.

KOLMES, E.J., OCHS, I.E., MLODIK, M.E., RAX, J.-M., GUEROULT, R. & FISCH, N.J. 2019 Radial current and rotation profile tailoring in highly ionized linear plasma devices. *Phys. Plasmas* **26** (8), 082309.

KOSTYUKOV, I.Y., SHVETS, G., FISCH, N.J. & RAX, J.M. 2002 Magnetic-field generation and electron acceleration in relativistic laser channel. *Phys. Plasmas* **9** (2), 636–648.

KRISHNAN, M., GEVA, M. & HIRSHFIELD, J.L. 1981 Plasma centrifuge. *Phys. Rev. Lett.* **46** (1), 36–38.

LEHNERT, B. 1970 A partially ionized plasma centrifuge. *Phys. Scr.* **2** (3), 106.

LEHNERT, B. 1971 Rotating plasmas. *Nucl. Fusion* **11** (5), 485.

LEHNERT, B. 1973 The partially ionized plasma centrifuge. *Phys. Scr.* **7** (3), 102.

LIZIAKIN, G., GAVRIKOV, A. & SMIRNOV, V. 2020 Negative electric potential in a cylindrical plasma column with magnetized electrons. *Plasma Sources Sci. Technol.* **29** (1), 015008.

LIZIAKIN, G., OILER, A., GAVRIKOV, A., ANTONOV, N. & SMIRNOV, V. 2021 Radial distribution of the plasma potential in a cylindrical plasma column with a longitudinal magnetic field. *J. Plasma Phys.* **87** (4), 905870414.

LOEB, A. & FRIEDLAND, L. 1986 Autoresonance laser accelerator. *Phys. Rev.* A **33** (3), 1828–1835.

MENDONÇA, J.T. 2012 Twisted waves in a plasma. *Plasma Phys. Control. Fusion* **54** (12), 124031.

NEZLIN, M.V. 1976 Negative-energy waves and the anomalous doppler effect. *Sov. Phys. Uspekhi* **19** (11), 946–954.

OCHS, I.E. & FISCH, N.J. 2017 Particle orbits in a force-balanced, wave-driven, rotating torus. *Phys. Plasmas* **24**, 092513.

OCHS, I.E. & FISCH, N.J. 2021a Nonresonant diffusion in alpha channeling. *Phys. Rev. Lett.* **127** (2), 025003.

OCHS, I.E. & FISCH, N.J. 2021b Wave-driven torques to drive current and rotation. *Phys. Plasmas* **28** (10), 102506.

OCHS, I.E. & FISCH, N.J. 2022 Momentum conservation in current drive and alpha-channeling-mediated rotation drive. *Phys. Plasmas* **29** (6), 062106.

OCHS, I.E. & FISCH, N.J. 2023 Ponderomotive recoil for electromagnetic waves. *Phys. Plasmas* **30** (2), 022102.

PENDERGAST, K., DANLEY, B., TEMKIN, R. & WURTELE, J. 1988 Self-consistent simulation of cyclotron autoresonance maser amplifiers. *IEEE Trans. Plasma Sci*. **16** (2), 122–128.

POULOS, M.J. 2019 Model for the operation of an emissive cathode in a large magnetized-plasma. *Phys. Plasmas* **26** (2), 022104.

PRASAD, R.R. & KRISHNAN, M. 1987 Isotope separation in a vacuum-arc centrifuge. *J. Appl. Phys*. **61** (9), 4464–4470.

RAX, J.M. 1992 Compton harmonic resonances, stochastic instabilities, quasilinear diffusion, and collisionless damping with ultra-high-intensity laser waves. *Phys. Fluids* B **4** (12), 3962–3972.

RAX, J.M. 2005 *Physique des plasmas*. Dunod.

RAX, J.-M. 2011 *Physique des tokamaks*. Ed. de l'Ecole polytechnique.

RAX, J.-M. 2021 *Mécanique Analytique*. Dunod.

RAX, J.M., GUEROULT, R. & FISCH, N.J. 2017 Efficiency of wave-driven rigid body rotation toroidal confinement. *Phys. Plasmas* **24** (3), 032504.

RAX, J.M., KOLMES, E.J., OCHS, I.E., FISCH, N.J. & GUEROULT, R. 2019 Nonlinear ohmic dissipation in axisymmetric DC and RF driven rotating plasmas. *Phys. Plasmas* **26** (1), 012303.

RAX, J.-M. & GUEROULT, R. 2019 Geometric phase in brillouin flows. *Phys. Plasmas* **26** (12), 122111.

RAX, J.-M. & GUEROULT, R. 2021 Faraday–Fresnel rotation and splitting of orbital angular momentum carrying waves in a rotating plasma. *J. Plasma Phys*. **87** (5), 905870507.

RAX, J.-M. & ROBICHE, J. 2010 Theory of unfolded cyclotron accelerator. *Phys. Plasmas* **17** (10), 103112.

RAX, J.-M., ROBICHE, J. & FISCH, N.J. 2007 Autoresonant ion cyclotron isotope separation. *Phys. Plasmas* **14** (4), 043102.

SHUKLA, P.K. 2012 Twisted shear alfvén waves with orbital angular momentum. *Phys. Lett.* A **376** (44), 2792–2794.

SHVETS, G., FISCH, N.J. & RAX, J.-M. 2002 Magnetic field generation through angular momentum exchange between circularly polarized radiation and charged particles. *Phys. Rev.* E **65** (4), 046403.

STENZEL, R.L. 2016 Whistler waves with angular momentum in space and laboratory plasmas and their counterparts in free space. *Adv. Phys.* X **1** (4), 687–710.

STENZEL, R.L. & URRUTIA, J.M. 2015 Helicon modes in uniform plasmas. III. Angular momentum. *Phys. Plasmas* **22** (9), 092113.

TEODORESCU, C., YOUNG, W.C., SWAN, G.W.S., ELLIS, R.F., HASSAM, A.B. & ROMERO-TALAMAS, C.A. 2010 Confinement of plasma along shaped open magnetic fields from the centrifugal force of supersonic plasma rotation. *Phys. Rev. Lett*. **105** (8), 085003.

THAURY, C., GUILLAUME, E., CORDE, S., LEHE, R., LE BOUTEILLER, M., TA PHUOC, K., DAVOINE, X., RAX, J.M., ROUSSE, A. & MALKA, V. 2013 Angular-momentum evolution in laser-plasma accelerators. *Phys. Rev. Lett*. **111** (13), 135002.

TIMOFEEV, A.V. 2014 On the theory of plasma processing of spent nuclear fuel. *Sov. Phys. Uspekhi* **57** (10), 990.

TROTABAS, B. & GUEROULT, R. 2022 Trade-off in perpendicular electric field control using negatively biased emissive end-electrodes. *Plasma Sources Sci. Technol*. **31**, 025001.

VORONA, N.A., GAVRIKOV, A.V., SAMOKHIN, A.A., SMIRNOV, V.P. & KHOMYAKOV, Y.S. 2015 On the possibility of reprocessing spent nuclear fuel and radioactive waste by plasma methods. *Phys. Atomic Nuclei* **78** (14), 1624–1630.

https://doi.org/10.1017/S0022377823000612 Published online by Cambridge University Press